Corrosion Behaviors of Structural Materials in Liquid Gallium and Gallium Alloy Environments for Nuclear Application

Sang Hun Shin

Interdisciplinary School of Green Energy
Graduate school of UNIST

Corrosion Behaviors of Structural Materials in Liquid Gallium and Gallium Alloy Environment for Nuclear Application

A thesis
submitted to the Interdisciplinary School of Green Energy
and the Graduate School of UNIST
in partial fulfillment of the
requirements for the degree of
Master of Science

Sang Hun Shin

01. 21. 2011
Approved by

_____
Major Advisor
Ji Hyun Kim

Corrosion Behaviors of Structural Materials in Liquid Gallium and Gallium Alloy Environments for Nuclear Application

Sang Hun Shin

This certifies that the thesis of Sang Hun Shin is approved.

01. 21. 2011

_____
Thesis Supervisor: Ji Hyun Kim

_____
Yonghee Kim: Thesis Committee Member #1

_____
In Cheol Bang: Thesis Committee Member #2

Abstract

Corrosion Behaviors of Structural Materials in Liquid Gallium and Gallium Alloy Environment for Nuclear Application

Sang Hun Shin

Interdisciplinary School of Green Energy
The Graduate School
Ulsan National Institute of Science and Technology

Liquid Metal Fast Breeder Reactor (LMFBR) is one of promising candidates among Gen IV nuclear energy systems. Among liquid metal, sodium is a spotlighted coolant material for designing fast breeder reactor. However, high activity of sodium with water and air is the major disadvantage that forces to search for alternatives. On the other aspects, the liquid metal including gallium generally interacts with structural materials, and it may cause Liquid-Metal-Embrittlement (LME) to materials in certain condition.

The purpose of this work is to examine the interaction between steels and liquid gallium or gallium alloys to evaluate the potential application of gallium for fast reactor coolants. In fact, gallium could be a good candidate for use as a liquid metal in the field of GEN IV nuclear system since it has low melting point (29°C), high boiling point (2204°C) and high safety against explosion. However, gallium has a high affinity for many metals and alloys, especially steels. For the prevention of liquid gallium corrosion with stainless steels, an active control of oxygen partial pressure which has been extensively studied for lead-bismuth corrosion could be adopted in this gallium environment.

The liquidus of gallium alloy (Ga-14Sn-6Zn and Ga-8Sn-6Zn) is 26°C and 19.5°C, respectively. Simultaneously, neutron absorption cross-section is reduced by these alloy process.

In this study, SS 316L and pre-oxidized specimens were exposed to static gallium and gallium alloys (Ga-14Sn-6zn and Ga-8Sn-6Zn) at 500°C for time up to 700 hr both in air and vacuum conditions ($5x10^{-6}$ torr). The results have shown that the corrosion resistance of pre-oxidized specimens was improved compared to bare specimens in

metal loss data. The weight change and metal loss were generally reduced in vacuum condition and also in gallium alloy environments. General behavior of developing reaction layer within the effect of pre-oxidation was that pre-oxidized specimens, in any conditions, had developed as thick as reaction layers on bare specimens.

Contents

I. Introduction

1.1 Background

For recycling spent fuels from operating nuclear power plant, liquid metal fast breeder reactor (LMFBR) is one of promising candidates among GEN IV nuclear energy system. Among liquid metals, sodium is a spotlighted coolant for designing fast breeder reactor. However the disadvantage of sodium, high activity with water and air, is the factor that searches for alternatives. This study suggests gallium as potential coolant for the next generation reactor. The element gallium possesses some of the requisites properties. It is a unique material, having a very low melting point, and a very high boiling point. It melts at 29°C, and suitable alloying might be capable of lowering the melting point to below room temperature. The boiling point is high, 2204°C. Being a liquid metal, the heat transfer characteristics would be good, though not so good as those some other liquid metals such as sodium [1]. However gallium has a high affinity for many metals and alloys, especially steels [1] and the absorption cross section of gallium is rather high, 2.2 barns per atom. This is a severe handicap, but since the cross section might be reduced by proper alloying.

The corrosion of structural metals and alloys in liquid gallium is for the most part due to the dissolution of various constituents of the metals or alloys by the liquid gallium. The unusual operating conditions of nuclear power reactors necessitate the use of unusual coolants. Thus, one desires a coolant which possesses a low cross section for absorbing neutrons, good heat-transfer efficiency, a low melting point and a high boiling point. Furthermore, a material which can contain the coolant, at the desire temperature, with insignificant rates of corrosion, is needed.

Since gallium had some promise as a reactor coolant, owing to its unique properties, research on the subject was merited. The research had as its objectives, determining the effect of alloying on melting point and on cross section, and studying the corrosion of possible container materials by gallium.

1.2 Objectives

For increasing power output of nuclear reactor, coolants need to be operated at higher temperature. Based on literature review, the number of published paper about gallium corrosion is not sufficient to know general corrosion behaviors of gallium at high temperatures. To investigate general gallium corrosion behavior with structural materials at higher temperature comparing to previously published papers [1, 2], corrosion tests are conducted in this thesis work.

The major issues of uses of gallium are listed below:

1) Relatively high neutron absorption cross-section
2) Relatively low thermal conductivity
3) Highly corrosive to some metals and alloys

The last one is primary issue to use gallium as a coolant.

The principal objective of this thesis is to develop protective oxide scale on the surface of specimens in gallium environment to prevent corrosion in widely used and commercially available structural alloys including stainless steels. For potential uses of gallium as a coolant, the corrosion issue has to be overcome.

REFERENCES

1. Jaffee, RI 1949, ‘Gallium in nuclear reactors: considerations for use as a primary coolant’, Battelle memorial institute,

2. Barier, F, ‘Corrosion of martensitic and austenitic steels in liquid gallium’,

3. Carre, F 2008, ‘Outlook on generation IV nuclear systems and related materials R&D challenges’, in V Ghetta(eds), Materials issues for generation IV systems, Springer

II. Literature Review

There are various requirements for nuclear structural materials, regardless of the exact reactor design or purpose of applications. The materials must be available and compatible. They must have good fabrication and joining properties. Good neutron transparency (low neutron absorption) is an important factor, especially for core applications such as fuel cladding and internal structures. The materials must have good mechanical properties at elevated temperature, including creep resistance, long term stability, and compatibility with the reactor coolant. Finally, since the materials will be used in a high-energy and high-intensity neutron field, it must be resistant to irradiation-induced properties changes (radiation hardening and Embrittlement, swelling, phase instability, creep).

In this chapter, major issues of structural materials for advanced fast reactor as well as corrosion issues in liquid gallium and gallium alloy will be reviewed.

2.1 Liquid Metal Embrittlement

Since liquid metals are considered as coolants for nuclear reactor, the Liquid Metal Embrittlement (LME) are one of issues that it makes hard to be used. The embrittlement of otherwise ductile metals stressed in contact with liquid metals has been known for at least sixty years. Despite its long history, however, it is still not well understood and laboratory experiments show that it is sensitive to both materials and testing conditions. Many materials are known to be susceptible. For example, ferrous alloys ranging from pure iron to austenitic stainless steels are variously reported to be embrittled by one or more of the liquid metals bismuth, gallium, mercury, indium, lithium, lead, tin and zinc [6, 7].

LME is the reduction in with elongation to failure that can be produced when normally ductile solid metals are stressed while in contact with a liquid metal. The prerequisite for LME is direct contact on an atomic scale between the stressed solid and the embrittler. This implies that the liquid must flow into any crack which may form and propagate. Direct experimental observations have shown liquid metal to penetrate to the tips of growing cracks [1]. Crack growth will stop if the supply of liquid is exhausted, except in the case of notch brittle materials if the critical flaw size has been exceeded. Similarly, interruption of the supply of the embrittling liquid leads to crack arrest in all but a few circumstances which will be commented upon later.

There are suggested theories to explain the mechanisms of LME. Theories have been proposed to explain failure by LME, suggesting mechanisms as diverse as increased air-pressure in pre-existing cracks [2], stress assisted dissolution, the weakening of inter-atomic bonds by the presence of a liquid metal at the crack tip, the formation of a weakly bonded alloy zone ahead of the crack tip, and enhanced plasticity at the crack tip [3]. Not all of these mechanisms, however, lead to predictions that compare well with experiment.

The most promising models at present are those that invoke weakening of the inter-atomic bonds in the solid at the crack tip. Such mechanisms have been referred to as "'adsorption-induced reduction in strength" by Kamdar as "adsorption-induced reduction in cohesion" as shown Fig. 2.1 [4]. Models based on reductions in energy values make it possible to interpret many of the characteristic phenomena of LME, but this approach has been contested by a thermally activated desorption of the embrittler atoms from the crack tip. This interpretation is consistent with the extensive deformation that precedes LME and the higher stresses needed for fracture than yielding, but it is unlikely that the very sharp transitions observed in some systems could be explained by the desorption mechanism [1].

And the effects of zinc and tin are considered. Clear evidence of separate nucleation and propagation

stages can be seen in the embrittlement of an AISI 4140 steel by zinc over a temperature range spanning the zinc melting point (260-422°C). At lower temperatures, many cracks were nucleated but propagation was slow, probably because the transport of the zinc to the crack-tip was limited to vapor or surface diffusion. As the temperature increased, progressively fewer cracks were formed until, above the melting point (419°C), only one crack was nucleated and propagated catastrophically in the presence of the liquid metal. Similar behavior occurred with lead, cadmium, tin and indium [5].

The presence of zinc on the fracture surface of ruptured stainless steel pipe work following a refinery accident in the US and the Flixborough disaster has been inter-preted as evidence of damage by LME. In both cases the suggested mechanism was the dripping of molten zinc from galvanized structures on to pipes which were stressed and at about 800°C due to a fire. The cost of damage that can be directly attributed to LME is difficult to estimate but may be substantial and therefore techniques for monitoring its onset before failure occurs and remedial action are of importance [1].

Since nuclear technology shared many materials and techniques with more conventional engineering, it is appropriate to consider the interaction or those factors which are peculiar to nuclear applications with the Embrittlement process.

2.2 Chemical compatibility of materials with liquid metal

2.2.1 Properties of gallium and liquid metals

Gallium is a unique material that has very wide range temperature existing as liquid state. Comparison with other coolant candidates as shown in Table 2.1, gallium has some advantages in low melting point, high boiling point, relatively high thermal conductivity, and chemical reactivity. However, gallium is a high neutron absorber that can adversely affect neutron economy in reactor physics design.

2.2.2 Solubility of elements in gallium and liquid metals

Corrosion of structural materials in contact with liquid gallium alloys occurs primarily as a simple dissolution process related to its solubility in the gallium. The solubility and corrosion of pure metals in gallium have been investigated [8, 9, 10]. The solubility and corrosion of pure metals are highly soluble in liquid gallium. Solubility of pure metals in gallium is based on a saturated solution in equilibrium with an intermetallic compound. The solubility of metal elements increases with increasing temperature. The solubility of Ni in gallium is higher than that of Cr and Fe as shown in Table 2.2 and Fig 2.2.

In order to direct comparison of solubility rate in contact with other liquid metal environments, solubility data of Ni, Cr, and Fe in lead and LBE are shown in Table 2.3~4 and Fig 2.3~4. Due to limited data, it is difficult to directly compare the results. The solubility of Ni in lead and LBE is higher than that of Ni in gallium. On the contrary, the solubility of Cr and Fe in gallium is higher than that of Cr and Fe in lead and LBE.

2.2.3 Corrosion behaviors of structural materials in gallium

Gallium has high affinity for many metals and alloys. The SS 316L austenitic steel specimens also showed significant corrosion at 400°C and developed a very thick compact reaction layer with time as shown Fig. 2.6. No preferential attack along the grain boundaries was observed [11].

It was decided that there were only four metals which showed promise [8, 9]. These metals are tantalum, tungsten, beryllium, and molybdenum [12]. Tungsten was found to be the most corrosion resistant of the available container metals for gallium at elevated temperature as shown in Fig. 2.7. When wet by gallium, tantalum shows attack at both 1000°F(538°C) and 1500°F(815°C), as may be seen in the micrograph in Fig. 2.8. Corrosion of molybdenum by gallium is severe at 1500°F. Heavy inter-metallic compound layers are formed, and considerable molybdenum goes into the liquid gallium by solution and by breaking off of the brittle compound formed. In some cases of longer exposure, intrusion of Ga-Mo compound into the molybdenum in radial directions, such as is shown in Fig. 2.9. This radial intrusion sometimes led to disintegration of the specimen. At 1500°F, gallium attack on beryllium was severe. The attack was inter-granular, and entire grains broke away from the beryllium surface. This made the beryllium surface irregular and the cross section no longer round as shown in Fig. 2.10. The general corrosion data of tungsten, tantalum, molybdenum, and beryllium are shown in Table. 2.6.

2.2.4 Comparison of protective oxide layer

The formation of protective oxide layer is one of the primary considerations that determine the durability of structural materials in liquid gallium. The key to good corrosion resistance is to establish an external, protective, and thermodynamically stable oxide phase. For high temperature applications, Cr_2O_3, Al_2O_3 and SiO_2 are the principal oxides used for the protection of metallic alloys. These oxides offer the potential for protection because the rates of metal and oxygen diffusion in the oxides are sufficiently low that they grow at an acceptably slow rate [13].

In J. Lim's work [19], thin Al_2O_3 layers were formed on the surface of all tested materials (Kanthal-AF®, MA956, PM2000) and there was no dissolution attack by lead bismuth eutectic (LBE). In the G. Muller's work [20], oxide layers on steels can effectively prevent the steel from leaching of alloy components by dissolution in liquid lead.

2.3 Principles of active control of oxygen in lead and LBE

Active oxygen control is an effective procedure to control the corrosion of structural materials in lead alloys. The role of oxygen is to form and maintain a self-healing protective oxide layer on the surface of structural materials [14]. The oxygen concentration in lead alloys should be maintained within a range between the dissociation limit of the oxide film (typically that of Fe_3O_4) and the saturation limit of Pb.

The low concentration of oxygen needed for the control technique makes it nearly impossible to supply oxygen at the right level directly. Such low level of oxygen can be achieved in certain reaction systems, e.g. hydrogen and water, or CO and CO_2 mixtures [15]. For versatility and safety reasons, hydrogen and water system is used for practical applications. The corresponding oxygen partial pressure can be calculated as following equation

$$p_{O_2} = \frac{p_{H_2O}^2}{p_{H_2}^2} \exp \frac{2\Delta_f G_{H_2O}^0}{RT}$$

with p_{O2}, p_{H2O}, and p_H being the oxygen, water, and hydrogen partial pressure in the gas phase, $\Delta_f G_{H_2O}^0$ as the standard Gibbs free energy of formation of water.

The Russian experience suggests that to avoid excess slagging in the process of using to passivate the

structural materials, a solid mass exchange device should be used. The mass exchanger consists of solid lead oxide (PbO) and liquid lead or LBE is controlled to have desired oxygen concentration. Oxygen concentration becomes equilibrium through dissolution of oxygen from solid lead oxide into liquid lead or LBE or oxide precipitates from liquid lead or LBE on the solid lead oxide and inner surface of the mass exchanger vessel [16, 17].

Table 2.1 Properties of liquid metal

Liquid Metal	Ga	Na	Pb	LBE
Atomic Number	31	11	82	-
Atomic Weight (amu)	69.72	23.0	207.2	~208
Melting Point (°C)	29	97.8	327.4	123.5
Boiling Point (°C)	2204	883	1750	1670
Density (kg/m^3)	6095	880	10500	10300
Thermal Conductivity (W/m-K)	40	76	16	11
Thermal Neutron Absorption Cross Section (Σ_a)	0.148	0.01347	0.005603	0.003034
Chemical Reactivity (with air and water)	Inert	Highly reactive	Inert	Inert

* Density and thermal conductivity are evaluated at 300°C.

Table 2.2 Solubility data in binary Ga-M systems [13].

Pure Metal	Coefficients of Equation		Solid Phase	Phase Stability Range (K)
	A	$B*10^{-3}$		
Cr	2.74	3.13	CrGa4	<298 – 973
Fe	4.00	3.85	FeGa3	<298 - 1097
Ni	2.52	1.85	NiGa4	-
Si	4.30	3.70	Si	<298 - 1687
W	4.90	8.75	WGa4	<298 - 3683

Table 2.3 Solubility data in binary Pb-M system [18]

Pure Metal	Coefficients of Equation		Phase Stability Range (K)
	A	$B*10^{-3}$	
Ni	2.78	1	<298 – 973
Cr	4.00	3.85	<298 - 1097
Fe	2.52	1.85	-

Table 2.4 Solubility data in LBE system [18]

Pure Metal	Coefficients of Equation		Phase Stability Range (K)
	A	$B*10^{-3}$	
Ni	2.74	3.13	<298 – 973
Cr	4.00	3.85	<298 - 1097
Fe	2.52	1.85	-

Table 2.5 Summary of data on corrosion of metals by gallium [12]

TABLE 3. SUMMARY OF DATA ON CORROSION OF METALS BY GALLIUM

Specimen	Diameter, in.	Weight, g.	Length of Test, hrs.	Temp., °F.	Wetted	Metal Pickup by Gallium, g (Spectro. Anal.)	Final Diam. Unreacted Metal, in.	Thickness Outer Reaction Layer, in.	Thickness Inner Reaction Layer, in.	Comments
Ta 5	0.080	0.3782	12	1500	Yes	< 0.05	0.079	0.0004	-	No visible reaction
Ta 10	0.080	0.3429	24	1500	No	< 0.05	0.078	0.0006	-	No visible reaction; specimen appeared dirty
Ta 11	0.080	0.3460	48	1500	Yes	ca 1.0	0.077	0.0008	-	Appears to have reacted slightly
Ta 12	0.080	0.3320	96	1500	Yes	ca 0.5	0.077	0.0010	-	No visible reaction
Ta 13	0.080	0.3468	96	1000	Yes	Not checked	0.080	0.0001	-	No visible reaction
Ta 11a	0.080	0.3311	48	1500	Yes	Not checked	0.078	0.0004	-	Slight reaction apparent (Ga-Sn-In alloy rather than pure Ga)
Mo 9	0.080	0.3065	24	1500	Yes	1-5	0.068	0.0052	0.0003	Appears to have reacted
Mo 10	0.080	Not weighed	48	1500	Partially	1-5	-	0.0400	-	Appears to have reacted; duplex alloy throughout
Mo 11	0.080	0.2953	96	1500	Yes	1-5	-	-	-	Appears almost completely reacted
Mo 12	0.080	0.2101	32	1500	Yes	1-5	0.030	0.0095	0.0037	Appears to have reacted; duplex alloy except for slight core
Mo 13	0.080	0.2102	96	1500	Yes	1-5	0.079	See comment	See comment	Appears to have reacted; duplex alloy throughout
Mo 14	0.080	0.2096	96	1000	Yes	Not checked	-	-	-	Appears almost completely reacted
Ti 7	0.080	0.0919	24	1500	Yes	0.5-<1.0	0.060	0.0024	0.0014	Partially reacted
Ti 8	0.080	0.0856	72	1500	Yes	0.5-<1.0	0.064	0.0042	0.0014	Appears to have reacted
Ti 9	0.080	0.0850	96	1000	Yes	Not checked	-	-	-	Completely reacted
W 2	0.080	0.4079	50	1500	Yes	0.001-0.005	0.083	None	-	No visible reaction
W 3	0.080	0.4083	96	1500	Yes	0.003-0.008	0.080	None	-	No visible reaction
W 4	0.080	0.4081	96	1000	Yes	Not checked	0.080	None	-	No visible reaction
Mo-61 1	0.088	0.2438	24	1500	No	No <.001; Si present	0.080	None	-	No visible reaction
Mo-61 2	0.088	0.2432	96	1000	No	Not checked	0.080	None	-	No visible reaction
Be 1	0.080	0.0378	12	1500	Yes	Not checked	0.061	0.0025	-	Appears to have reacted; capsule brown-black inside
Be 2	0.079	0.0359	25	1500	Yes	Ditto	0.061	0.0033	-	Appears to have reacted; capsule brown-black inside
Be 3	0.079	0.0360	48	1500	Yes	"	0.055	0.0050	-	Reacted; capsule brown-black inside
Be 4	0.080	0.0360	96	1500	Yes	"	0.038	0.0083	-	Reacted; capsule brown-black inside
Be 5	0.080	0.0359	96	1000	Yes	"	0.076	None	-	No visible reaction

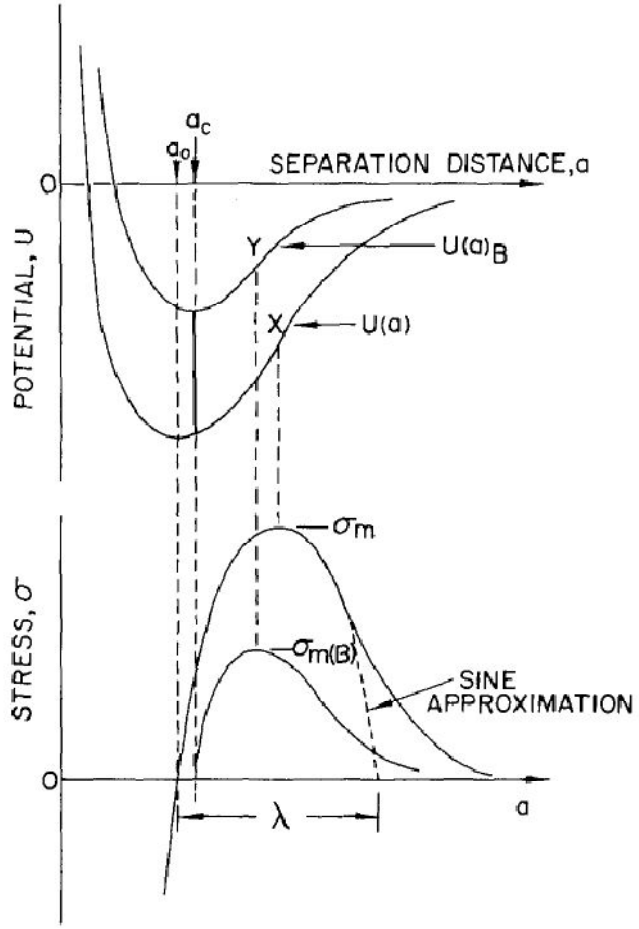

Fig. 2.1 Schematic potential energy, U(a) and $U(a)_B$, and resulting stress, σ(a) and $\sigma(a)_B$, versus separation distance curves in the absence and presence of chemisorbed atom B. For spontaneous chemisorptions of B, $a_c=a_0$ [4].

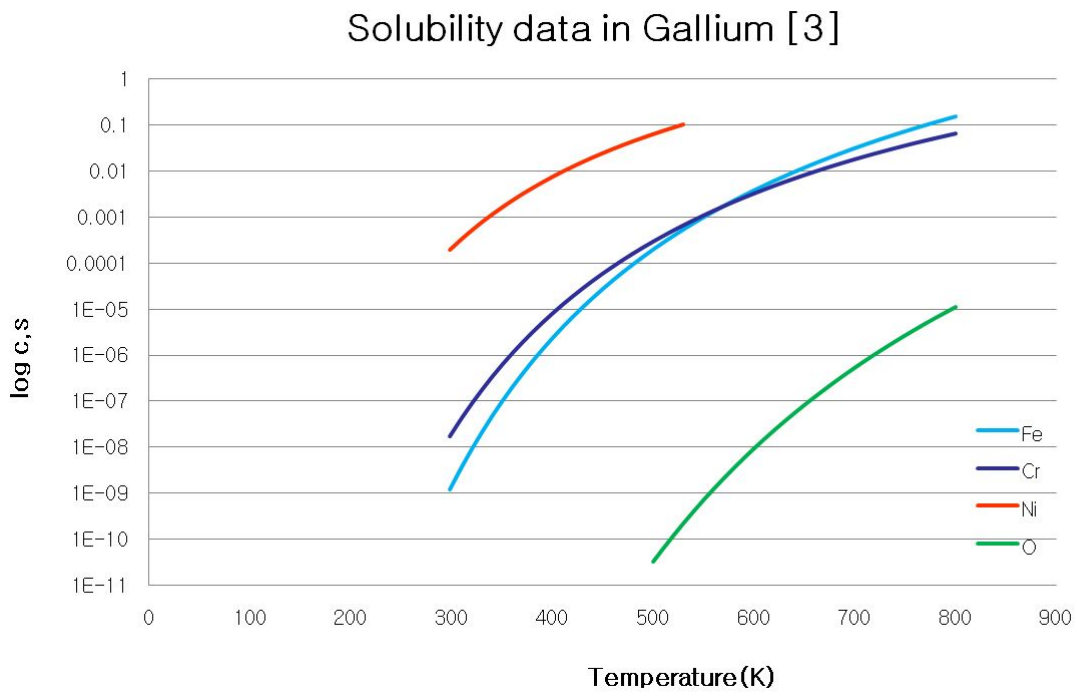

Fig. 2.2 Solubility data of major elements of SS 316L in gallium [3]

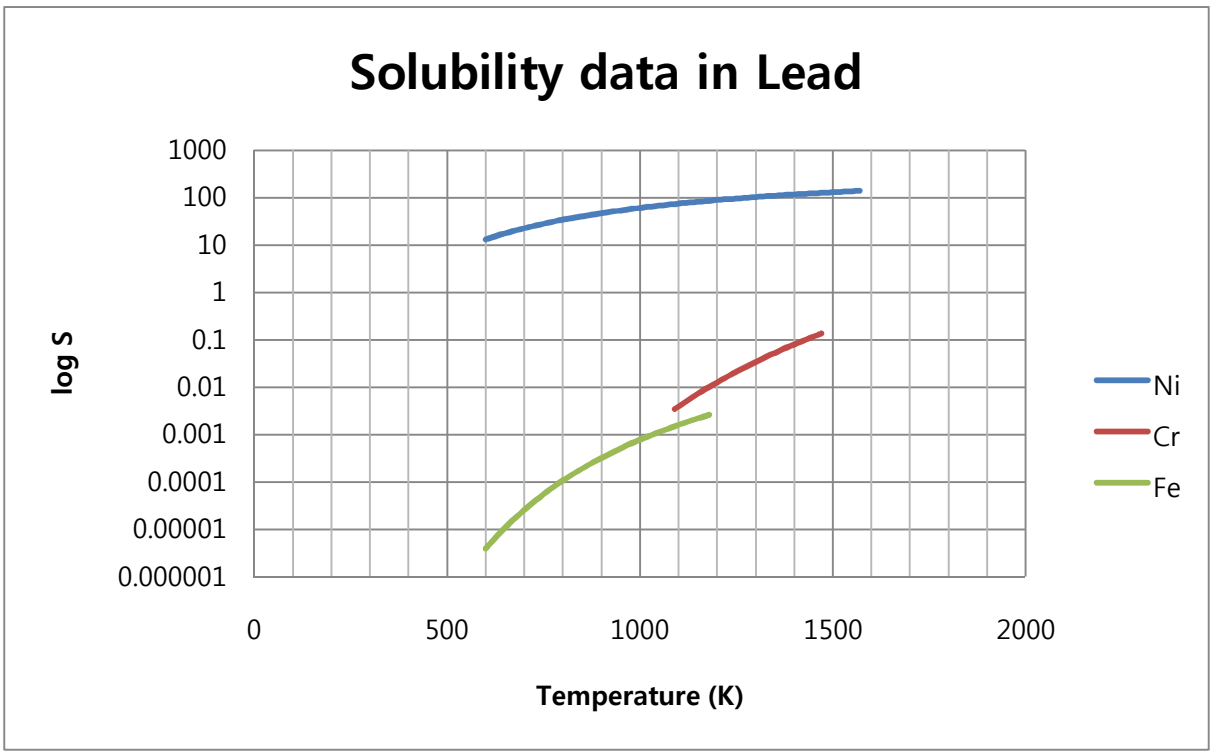

Fig. 2.3 Solubility data of major elements of SS 316L in gallium [18]

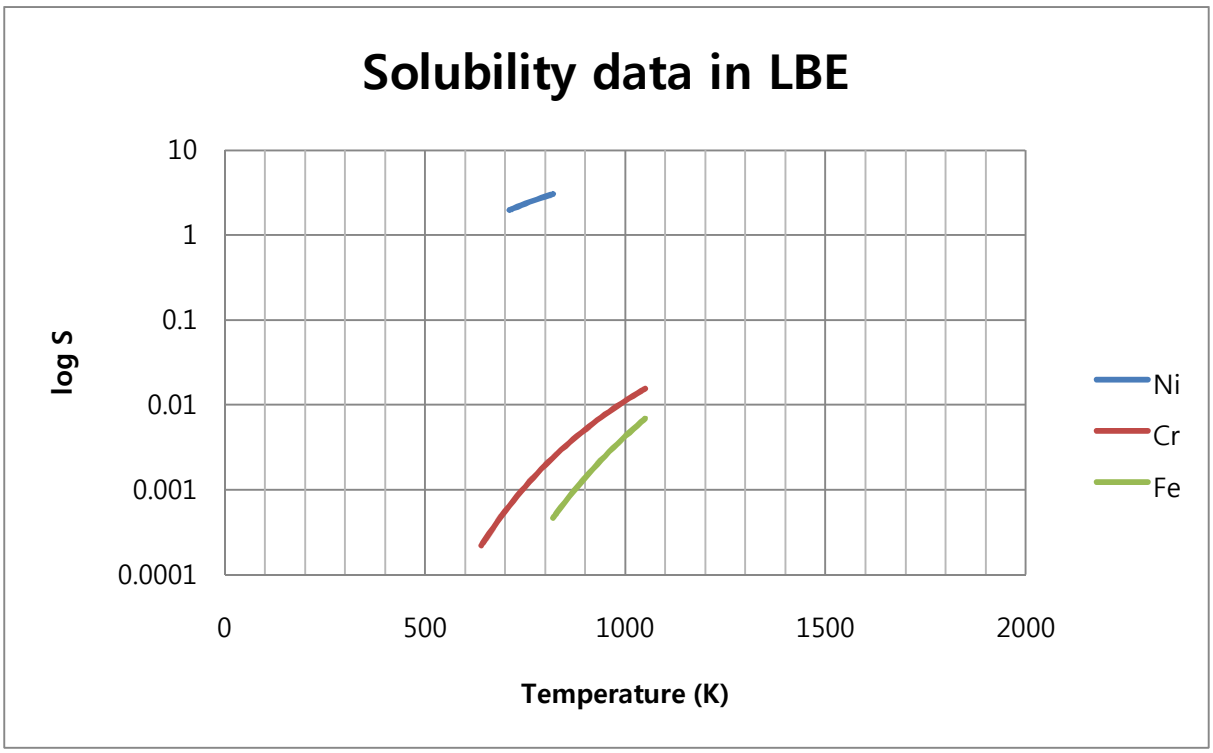

Fig. 2.4 Solubility data of major elements of SS 316L in gallium [18]

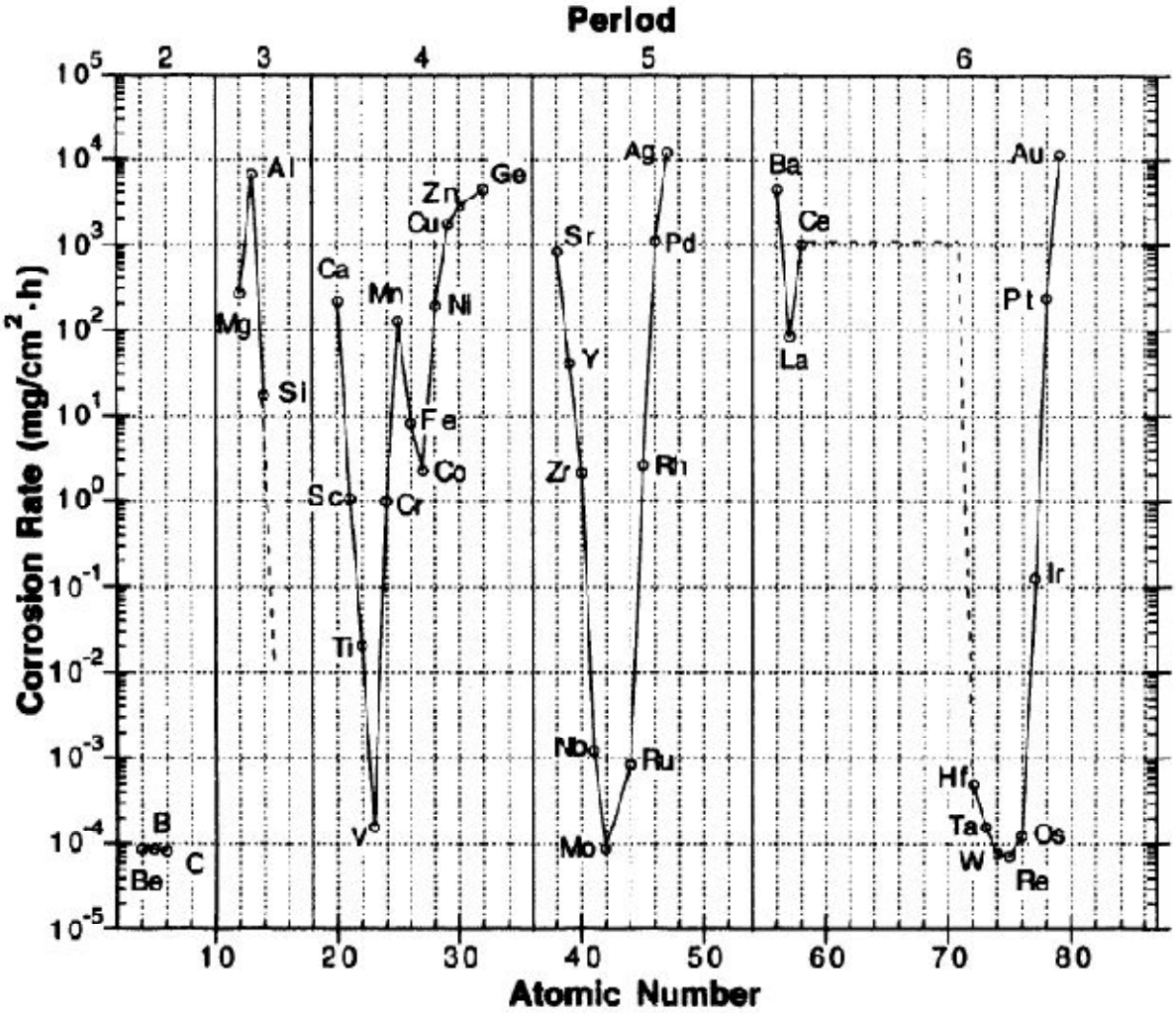

Fig. 2.5 Periodicity of corrosion rate of metals in liquid gallium at 400°C [13]

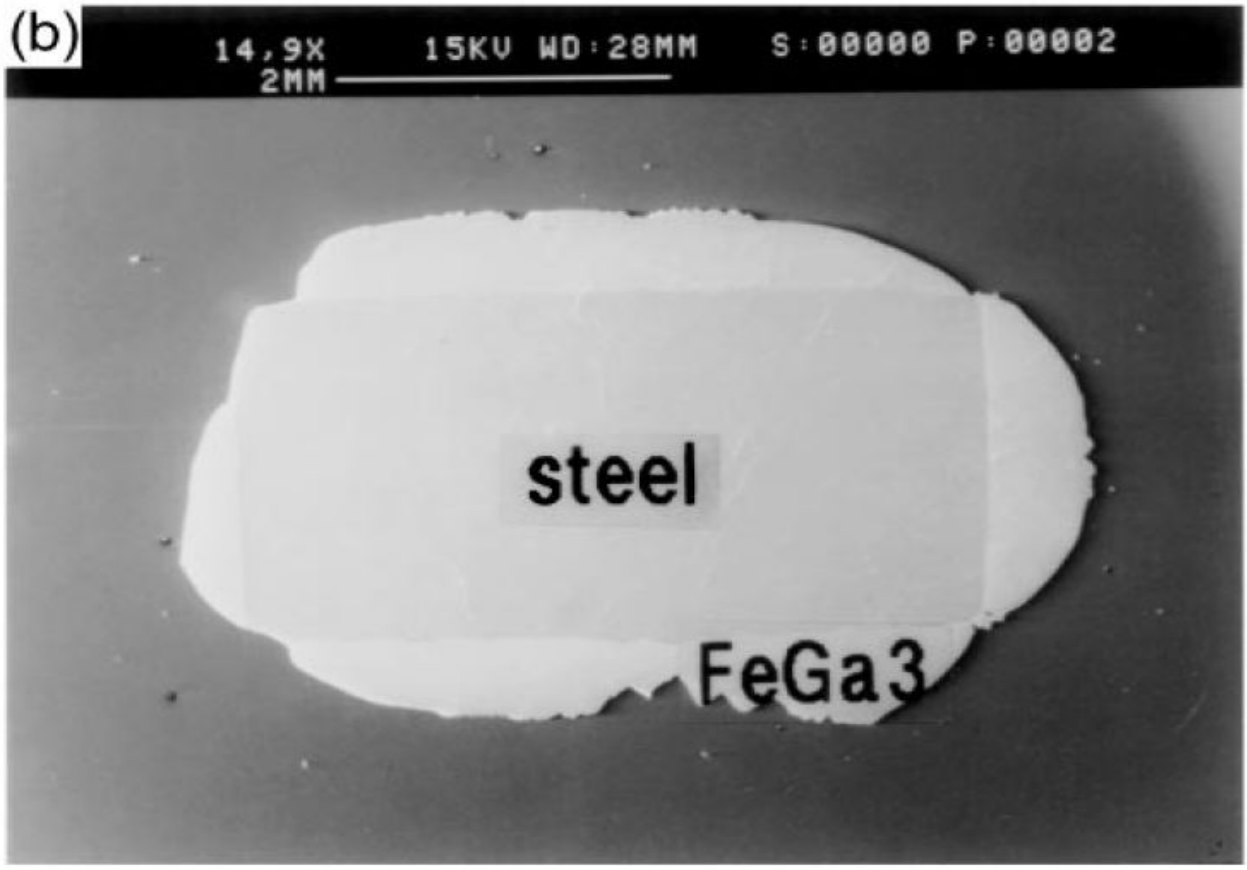

Fig. 2.6 Cross section of 316 L austenitic steel specimen exposed to gallium at 400°C for 307 hr [11]

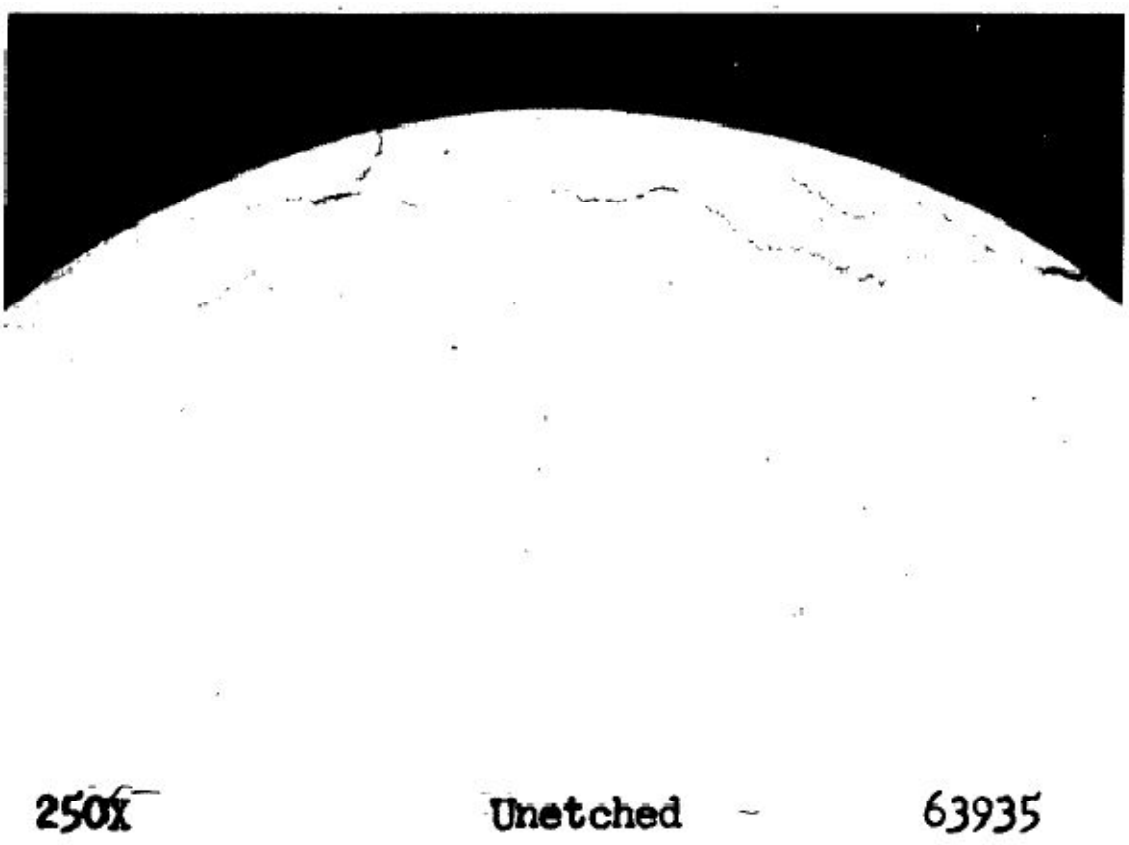

Fig. 2.7 Micrograph of tungsten rod after immersion in gallium for 48 hours at 1500°F (Crack shown were formed during sectioning, and are not evidence of corrosion attack) [12]

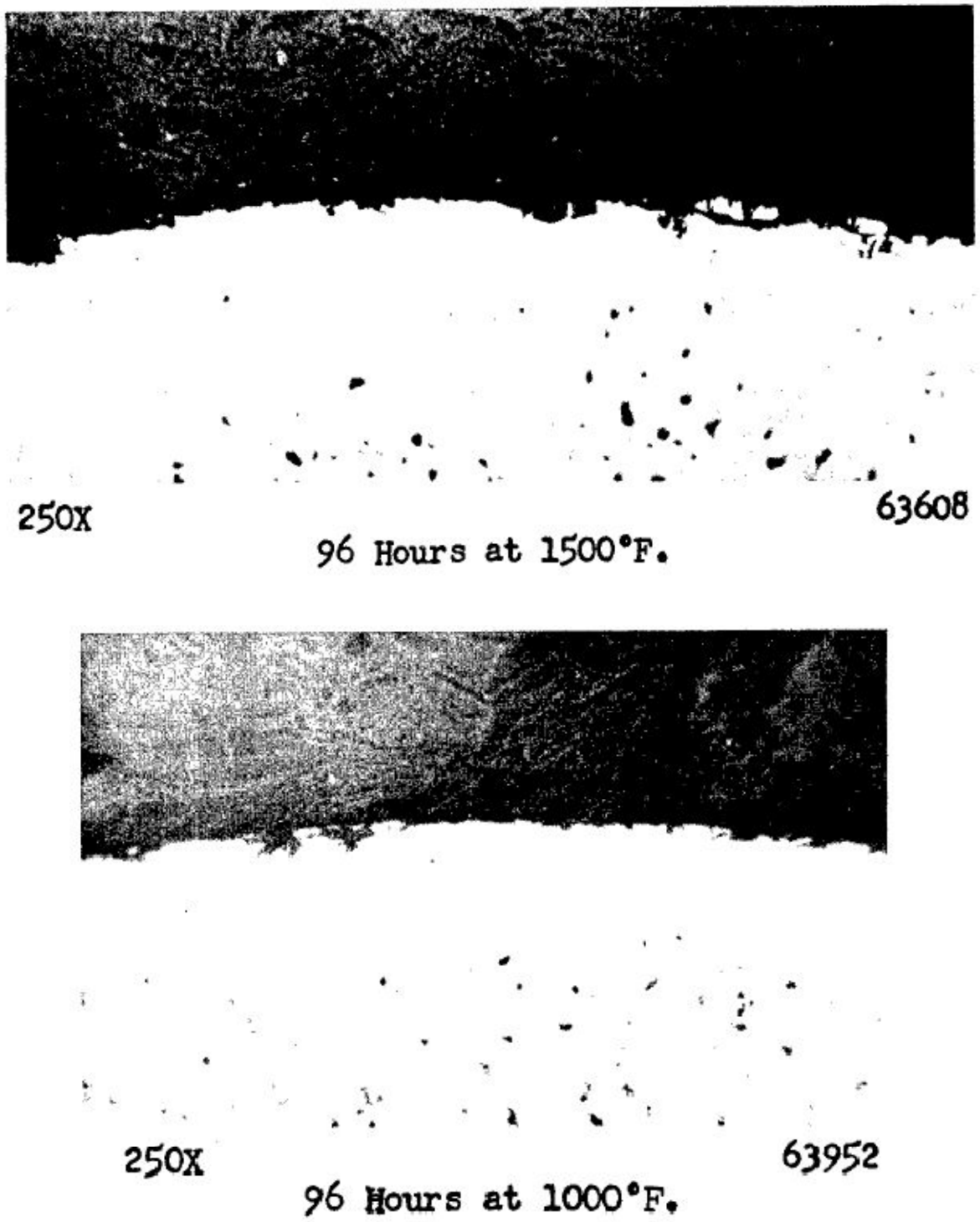

Fig. 2.8 Micrograph of tantalum rods after immersion in gallium for 96 hours at 1500°F and 1000°F [12]

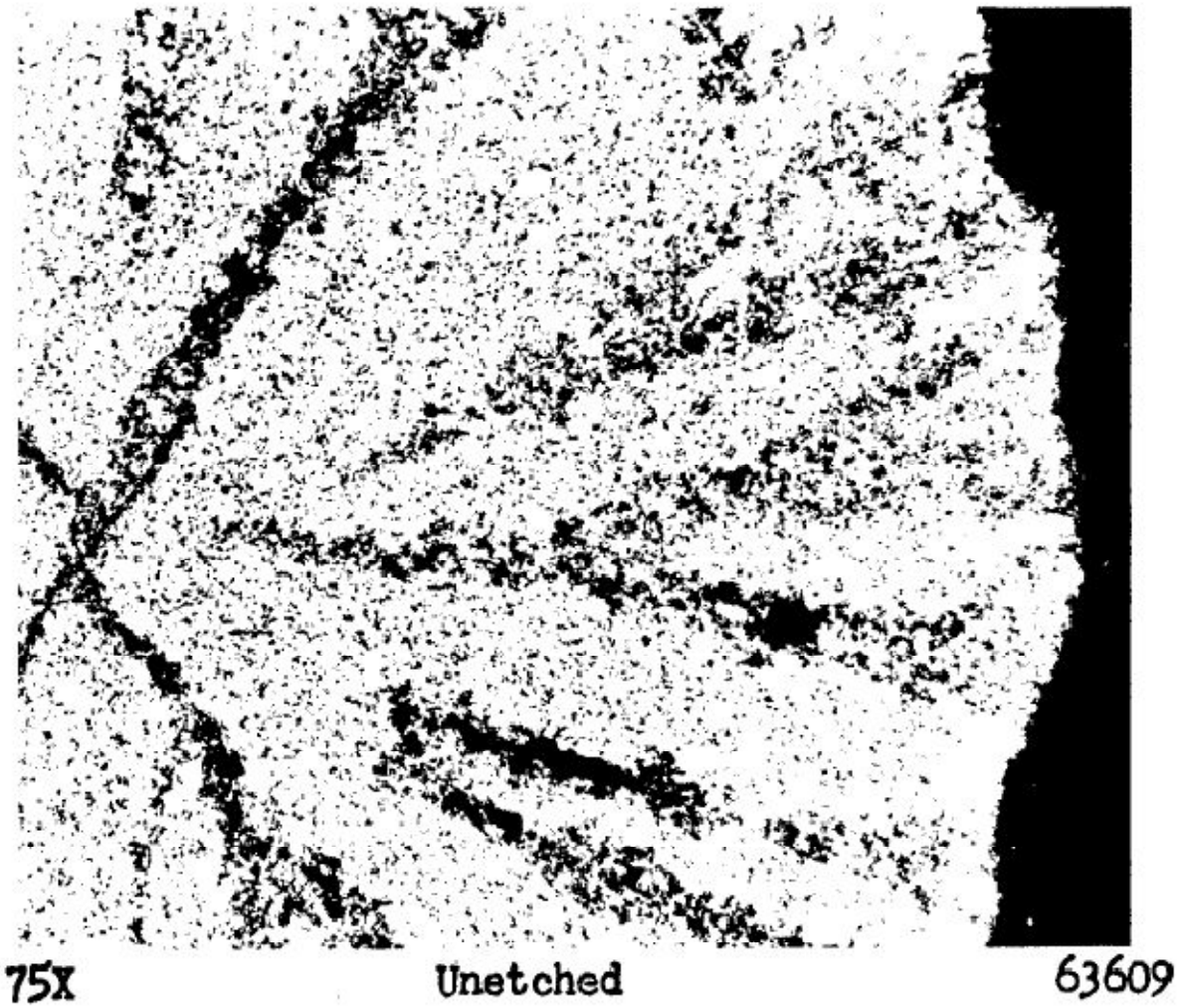

Fig. 2.9 Micrograph of molybdenum rod after immersion in gallium for 48 hours at 1500°F [12]

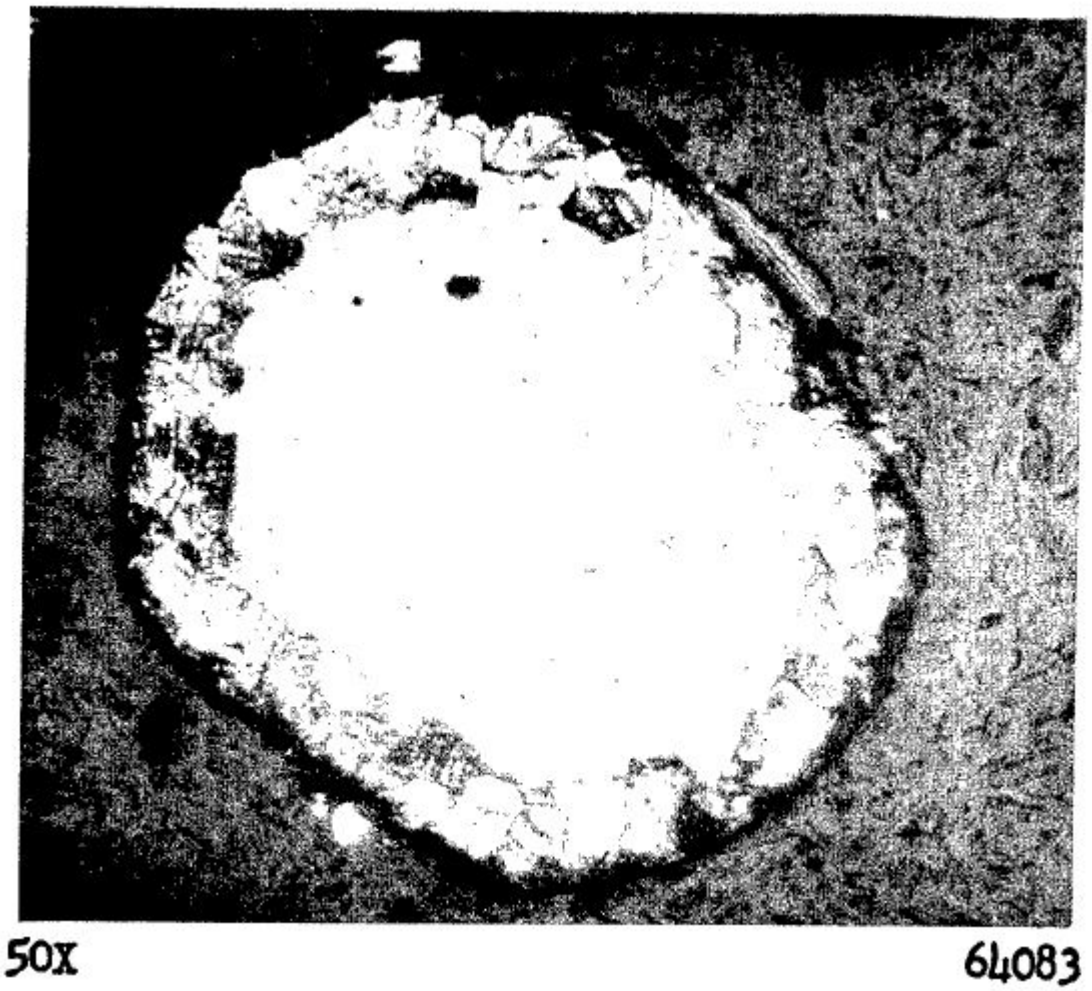

Fig. 2.10 Micrograph of beryllium after immersion in gallium for 96 hours at 1500°F, etched with dilute HNO_3-HF [12]

REFERENCES

1. Nicholas, M. D & Old, C. F 1979, Review: Liquid Metal Embrittlement, *Journal of Science,* vol. 14, 1-18

2. Makin, M. J 1958, in: Proceedings of 2nd UN international Conference on Peaceful Uses of Atomic Energy, Vol. 5, 446

3. Lynch, S. P 1977, in: Proceeding of 4th International Conference on Fracture, Vol. 2, 859

4. Kamdar, M. D 1973, Embrittlement by Liquid Metals, *Progress in Materials Science*, vol. 15, 289-374

5. Old, C. F 1980, Liquid Metal Embrittlement of Nuclear Materials, *Journal of Nuclear Materials,* vol. 92, 2-25

6. Tanaka, M & Fukunaga, H 1969, Fatigue Strength of Mild Steel. 13 Cr and 18 Cr-8 Ni Steel Subjected to Elevated Temperatures and to Contact with Liquid Pb and Sn, *Journal of the Society of Materials Science (Japan),* vol. 18, 254-258

7. Coleman, E. G., Weinstein, D. & Rostoker, W 1961, On a Surface Energy Mechanism for Stress-Corrosion Cracking, *Acta Metallurgica,* vol. 9, 491-496

8. Wilkinson, W. D 1953, Effects of Gallium on Materials at Elevated Temperatures, *Argonne National Laboratory Report ANL-5027*

9. Wilkinson, W. D 1953, Effects of Gallium on Materials at Elevated Temperatures Supplementary Report, *Argonne National Laboratory Report ANL-4582*

10. Bailar, J. C., Emeleus, H. J., Nyholm, R. & Trotman-Dickenson, A. F 1973, Comprehensive Inorganic Chemistry, *Pergamon Press,* Oxford, U. K., 993-1007

11. Barbier, F. & Blanc, J 1999, Corrosion of Martensitic and Austenitic steels in Liquid Gallium, *Journal of Materials Research,* vol. 14, 737-744

12. Jaffee, R. I., Evans, R. M., Fromm, E. A. & Gonsor, B. W 1949, Gallium in Nuclear Reactors: Considerations for Use as a Primary Coolant, *Battelle Memorial Institute AECD-3317*

13. Luebbers, P. R., Michaud, W. F. & Chopra, O. K 1993, Compatibility of ITER Candidate Structural Materials with Static Gallium, *Argonne National Laboratory ANL-93/31*

14. Ning, L 2002, Active control oxygen in molten lead-bismuth eutectic systems to prevent steel corrosion and coolant contamination, *Journal of Nuclear Materials,* vol. 300, 73

15. Gaskell, D. R 2003, Introduction of the thermodynamics of materials, 4th edition, *Taylor & Francis*

16. Ning, L 2008, Lead-alloy coolant technology and materials-technology readiness level evaluation, *Progress in Nuclear Energy,* vol. 50, 140-151

17. Kondo, M., Takahashi, M., Miura, K. & Onizawa, T 2006, Study on control of oxygen concentration in lead-bismuth flow using lead oxide particles, *Journal of Nuclear Materials,* vol. 357, 97-104

18. Handbook of lead-bismuth eutectic alloy and lead properties, material compatibility, thermal hydraulics and technologies, *OECD-NEA*, 2007

19. Lim, J 2010, A study of early corrosion behaviors of FeCrAl alloys in liquid lead-bismuth eutectic environment, *Journal of Nuclear Materials,* vol. 407, 205-210

20. Muller, G 2000, Investigation on oxygen controlled liquid lead corrosion of surface treated steels, *Journal of Nuclear Materials,* vol. 278, 85-95

III. Rationale and Approach

3.1 Problem definition

Since 1950s, researchers studied the use of gallium as coolants and expected that it is unique material for this application. But the significant corrosion at elevated temperature in some metals and alloys were observed. The most compatible materials interacted with gallium at high temperature were known as refractory metals such as tungsten. But the difficulty of manufacturing process of refractory metals was one of issues to use them in gallium environment.

Meanwhile, austenitic stainless steels have good mechanical properties as structural materials. However, as reviewed in Chapter II, SS 316L also severely corrodes by gallium at 400°C. To increase thermal efficiency it is necessary to increase operating temperature. So, it is necessary to conduct corrosion tests of gallium at higher temperature. In this thesis, all corrosion tests have been conducted at 500°C.

If the corrosion resistance of SS 316L in gallium is guaranteed for designed life of system, it can be adopted as a good structural material in gallium environment. For the prevention of liquid gallium attack to stainless steels, an active control of oxygen partial pressure which has been extensively studied for preventing lead-bismuth corrosion with structural materials can be adopted in gallium environment.

3.2 Goal

Based on fast reactor structural material requirements, the principal goal of this thesis is to develop protective oxide scale on the surface of SS 316L in gallium environments at high temperature for nuclear application.

Detail objectives of this thesis work are defined as follows:

- To investigate general corrosion behavior of structural materials such as SS 316L in gallium and gallium alloy environments at 500°C
    - Corrosion behavior of bare metal in gallium and gallium alloy environments at 500°C
    - Corrosion behavior of pre-oxidized (surface oxidation) sample in gallium and gallium alloy environments at 500°C
    - Corrosion behavior of SS 316L and pre-oxidized 316 L in actively oxygen controlled environment

3.3 Approach

To see the corrosion behavior of SS 316L in gallium and gallium alloys, a interface between base metal and inter-metallic compound formed on the surface was investigated and analyzed as shown in Fig. 3. 1 and considered as blow:

- Corrosion behavior of SS 316L in liquid gallium at 500°C tested in air and vacuum
- Effects of pre-oxidation on corrosion behavior
- Quantitative analysis (Electron probe micro-analyzer : EPMA) and line-profiling analysis (Energy dispersive spectrometry : EDS and EPMA)

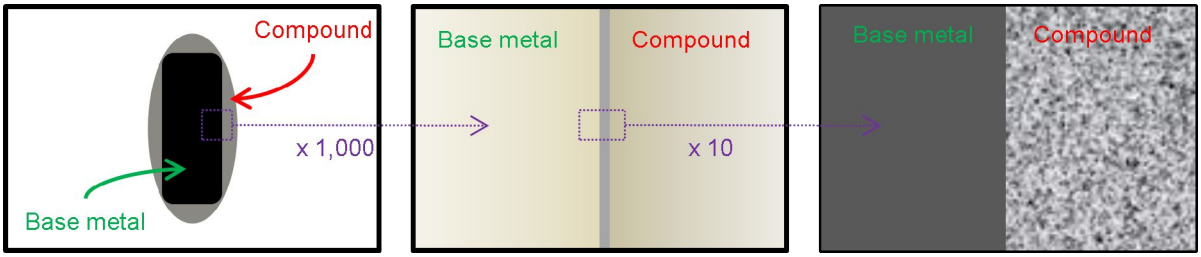

(a) (b) (c)

Fig. 3.1 Experimental approach to investigate corrosion behaviors in interesting region of SS 316L, (a) optical image (low magnitude), (b) optical image (high magnitude), and (c) SEM image

IV. Experimental

4.1 Specimen preparation

In this study, SS 316L was exposed to static gallium and gallium alloy at 500°C for up to 700 hrs. All specimens for corrosion test with dimensions of 30 mm in length, 10 mm in width and 3 mm in thickness were cut by high pressure water jet process to avoid thermal stress. Prior to exposure in gallium, each specimen was mechanically polished by SiC papers, diamond suspension(6μm, 3μm, and 1μm), and finally alumina paste down to 0.04μm, then ultrasonically cleaned with water for 30 min. Some specimens were pre-oxidized with three different conditions. Specimens were pre-oxidized at 500°C air for 24 and 100 hr, and at controlled O_2 for 24 hr, respectively. Each specimen was put into alumina crucible for avoiding precipitate from container. Tests were conducted at air and high vacuum furnace shown in Figs. 4.1~2.

To primarily prevent corrosion, specimens were pre-oxidized under three conditions as shown in Fig. 4.5. First was that specimen was exposed to 500°C air for 24 hrs, second was the same condition but longer time (100 hrs). The last condition was that specimen was exposed to primarily high vacuum condition and then the furnace was filled with 500°C controlled O_2 for 24 hrs for the formation of Cr_2O_3 only on the surface of specimen described in Table. 4.2 and specific H_2/H_2O ratio was controlled to 135,000 corresponding to $1.356*10^{-38}$ atm of oxygen partial pressure(p_{O2}).

4.2 Experimental system description

Experimental system for actively controlling oxygen partial pressure, mass flow controller (MFC), liquid flow meter (LFM), and control evaporation mixer (CEM) were equipped as shown in Fig. 4.3. The two MFCs are for mass control of argon and hydrogen gas, respectively. To obtain optimized oxygen partial pressure in this work, 0.2 cc/hr of water was controlled by LFM. Then, this controlled water come in CEM to be evaporated and mixed with two gases from MFCs. The heating temperature in CEM was set into 200°C. And SS 316L tube lines are connected from CEM outlet to gallium cells inlet. These tube lines also are heated by heating wire to keep temperature up to 200°C. It is important for water vapor among the fluids flowing in tubes not to be condensed.

The standard Gibbs free energy change data for the oxidation of selected solid metals are listed in Table. 4.2, along with their equilibrium oxygen partial pressure values. As a way to set oxygen partial pressure at a desired level, the well established method of controlling the ratio of the partial pressure of gaseous hydrogen with to moisture content is applicable for liquid gallium systems. Fig. 4.4 shows an Ellingham diagram for selected materials, depicting the domain of thermodynamic stability of their oxides in terms of temperature and oxygen partial pressure. Lines indicating constant $p(H_2)/p(H_2O)$ ratios are superimposed for comparison purposes. This type of diagram offers a useful way to estimate the equilibrium condition of a metal/metal oxide. With the assumption of thermodynamic equilibrium, one can use this diagram to determine the required partial pressure ratio of hydrogen and moisture to oxidize certain metal-oxide/metal systems.

The condition to form chromium oxide is to set the oxygen partial pressure between $1.483*10^{-38}$ and $3.71*10^{-42}$ atm in the static gallium cells by oxygen control system as described above. As discussed in the previous chapter, controlling the oxygen potential is critical to development of a fundamental understanding on the corrosion phenomena of structural materials in contact with liquid gallium or gallium alloys.

An alumina crucible was used as the gallium container in each oxygen-controlled cell.

4.3 Testing and analysis procedures

Basically, austenitic stainless steel specimens were tested in liquid gallium and gallium alloy environments at 500°C. After testing, the tested specimens were removed from alumina crucible and were washed in warm water at about 50°C to primarily residual gallium, then ultrasonically cleaned with water at 50°C for one hour. Then the specimens were cold-mounted using mixture of epoxy resin and hardener. To examine cross-section of mounted specimens, they were cut using low speed saw, then cross-section area were polished with SiC paper with water down to 1200 grit, and with 6, 3, and 1 μm diamond suspension. Final surface preparation was polished with 0.04 μm alumina pastes. Specimens proceed with this surface finish were examined using scanning electron microscopy (SEM) after carbon coating.

Table 4.1 Chemical composition of SS 316L

Element	Fe	Cr	Ni	Mo	Mn	Si	Other
wt(%)	Bal.	16.43	10.05	2.02	1.02	0.66	-

Table 4.2 Thermodynamic conditions for the formation of Cr_2O_3 only on the surface of specimen

Oxides	ΔG (J/mol)	H_2/H_2O ratio	P_{O2}(atm)
Ga_2O_3	**-840,000**	**$1.2818*10^5$**	**$1.483*10^{-38}$**
Cr_2O_3	**-987,502**	**$2.6863*10^8$**	**$3.71*10^{-42}$**

Fig. 4.1 Photograph of air furnace for corrosion test

Fig. 4.2 Photograph of high vacuum furnace for corrosion test

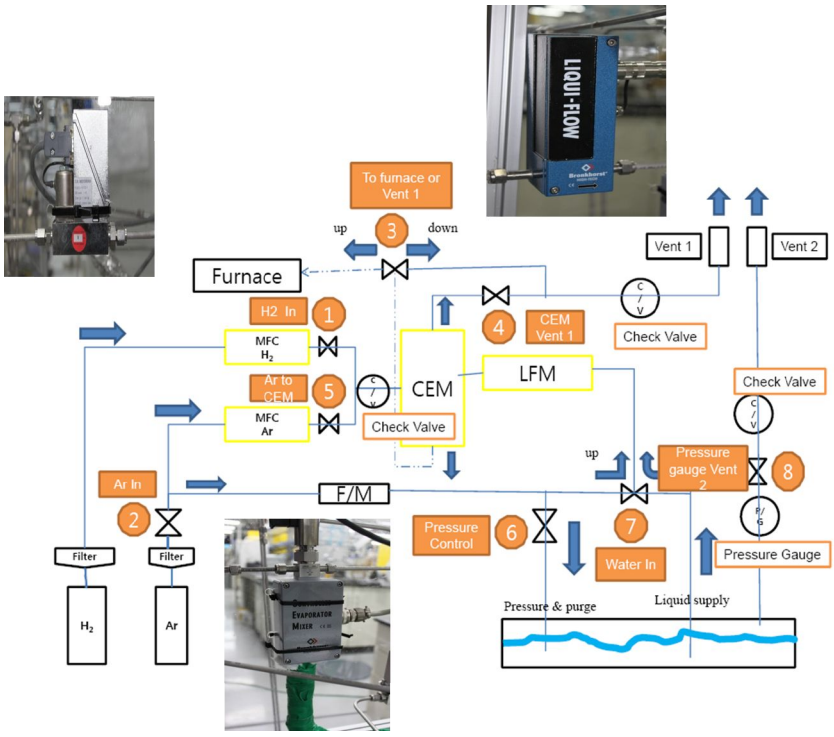

Fig. 4.3 Schematics of oxygen control system

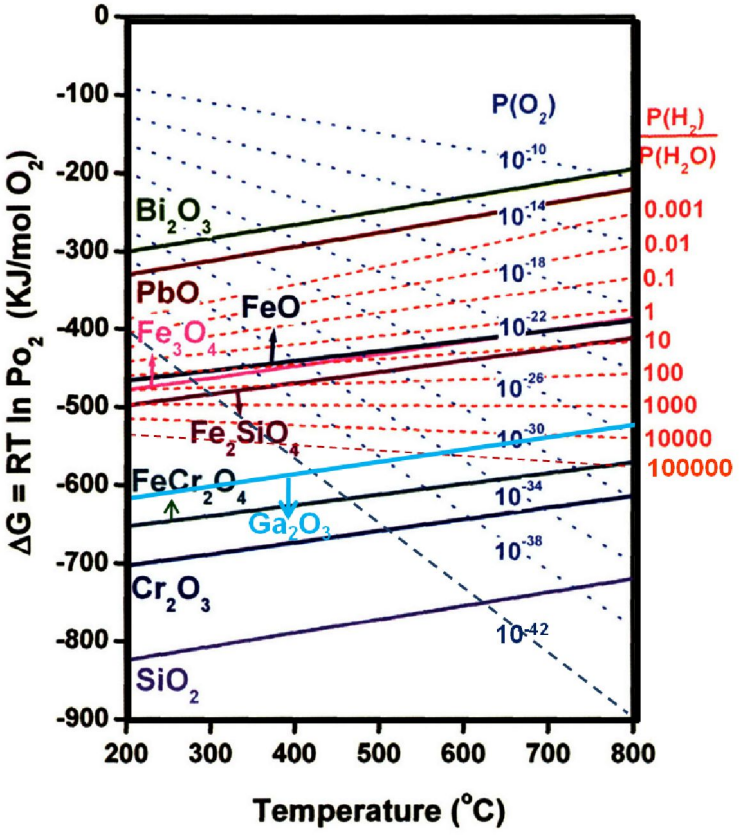

Fig. 4.3 Ellingham diagram for selected metal-metal oxide systems [4].

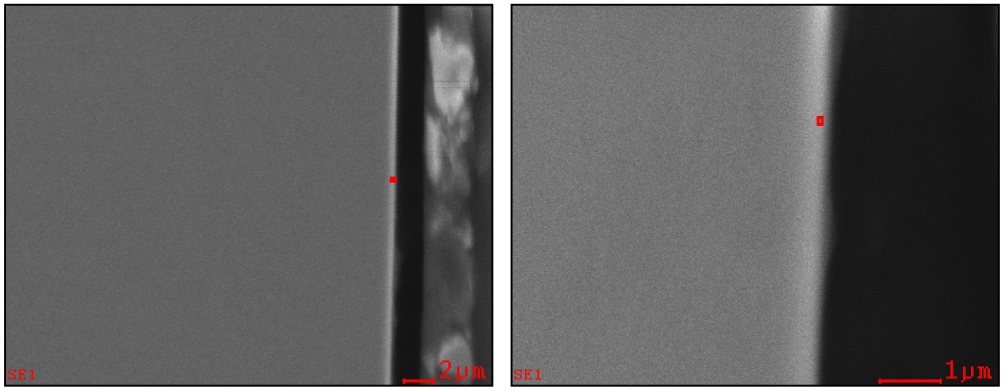

(a) (b)

Element	Wt%	At%
OK	02.94	09.54
FeL	62.46	58.02
NiL	18.23	16.11
CrK	16.37	16.33
Matrix	Correction	ZAF

Element	Wt%	At%
OK	03.59	11.28
FeL	51.24	46.13
NiL	09.76	08.36
CrK	35.41	34.23
Matrix	Correction	ZAF

Fig. 4.3 SEM images of surfaces on the specimens (a) pre-oxidized at 500°C air for 24 hr and (b) pre-oxidized at 500°C controlled O_2 for 24 hr, and EDS analysis of small rectangle regions.

REFERENCES

1. Luebbers, PR 1993, ‘Compatibility of ITER candidate structural materials with static gallium’, Argonne National Laboratory, U.S DOE

2. Yatsenko, SP 1970, ‘Solubility of metals of fifth period in liquid gallium’, Sov. Mater. Sci., Vol. 6

3. Prokhorenko, V 2000, ‘Liquid gallium: potential uses as a heat-transfer agent’, High temperature, Vol. 38,

4. Jeongyoun, L 2006, ‘Effects of chromium and silicon on corrosion of iron alloys in lead-bismuth eutectic’, Thesis of Doctor of Science in Nuclear Science and Engineering, MIT

V. Results

5.1 Morphology and composition of reaction layer

After exposure to gallium and gallium alloy, the specimens were mounted, sectioned, and polished for metallographic examination. As increasing with exposure time to gallium, the volume of specimens were smaller, thickness of reaction layer was thicker, and weight loss was higher. Generally for all specimens shown in Figs. 4.1~5, the thickness of reaction layer was not the same for all sides of the specimens because reaction layer dominantly formed to width direction with time.

5.2 Corrosion behavior

The weight change, metal loss, and reaction layer of specimens found after exposure to gallium and gallium alloys are plotted as a function of times up to 700 hr. All, bare metal, pre-oxidized at 500°C air for 24hr, pre-oxidized at 500°C air for 100hr, and pre-oxidized at 500°C controlled O_2, specimens were showing different metal loss, weight change, and reaction layer data. Also, corrosion environments (pure gallium and gallium alloy) have an effect on corrosion behaviors.

5.2.1 Weight change

The definition of weight change is as below:

$$\frac{\Delta\text{weight (after} - \text{before exposure)}}{\text{surface area}} \left[\frac{\text{mg}}{\text{cm}^2}\right]$$

Before exposed to gallium, the weight of all specimens was measured. After testing, the specimens were first washed in a 50°C water to remove gallium adhering to the surface, and then ultrasonically cleaned in DI water to ensure complete removal of gallium. After drying, the specimen weight was measured.

After bare specimens exposed to gallium for 700 hr in air and vacuum, the weight changes are -804.32 mg/cm^2 and -658.7 mg/cm^2, respectively as shown in Figs. 4.6 and 4.7. The weight change of specimens tested in controlled O_2 for 307 hr is -297.4 mg/cm^2. For Bare specimens tested in same conditions but under gallium alloy environment (Ga-14Sn-6Zn), the weight changes are -458.9 mg/cm^2(air condition) and -238.9 mg/cm^2(vacuum condition), respectively. Under different composition of gallium alloy (Ga-8Sn-6Zn), the weight changes of bare specimens are -324 mg/cm^2 (air) and -331.7 mg/cm^2 (vacuum), respectively. The tendency at here is that bare specimens tested in air condition undergo higher weight changes compared to vacuum condition. Other pre-oxidized specimens also clearly show this tendency as shown in Figs. 4.6~4.11.

The weight changes of bare specimen, pre-oxidized specimen with gallium, and bare specimens with gallium alloy (Ga-14Sn-6Zn) tested in controlled O_2 for 307 hr are -297.4 mg/cm^2, -46.5 mg/cm^2, and -166.23 mg/cm^2, respectively as shown in Fig. 4.12.

5.2.2 Reaction layer

At this thesis work, 30 sections in thickness of reaction layer were measured, and then the averaged values were recorded in each specimen. Because increasing exposure time, the reaction layer

parabolically grew up as shown Figs. 4.1~4.5.

The mechanisms of forming reaction layer is that main constituents of stainless steel is soluble in gallium, when they meet gallium at high temperature, the compound start to form on the surface. These figures and graphs from Fig. 4.26 to 4.35 show SEM images and EPMA quantitative analysis at the interface in depth with 40 um. At steel region, iron, nickel, and chromium′s signal is dominant. At reaction layer region, gallium, iron, chromium, and nickel iron are mixed and formed compound.

After exposure to gallium for 700 hr in air and vacuum, the thickness of reaction layer of bare specimens is 637μm, 583.2μm, respectively. In gallium alloys environments, the thickness is 508μm (air), 493μm (vacuum) in Ga-14Sn-6Zn and 475μm (air), 552.5μm (vacuum) in Ga-8Sn-6Zn, respectively. For the bare metals, there is also tendency that the thickness of reaction layer is thin at vacuum condition compared to air condition but not Ga-8Sn-6Zn environment.

Specimens that pre-oxidized at 500°C controlled O_2 for 24hr developed a very thick reaction layer both air and vacuum conditions shown in Figs. 4.13~14. The specimens exposed to 500°C gallium exhibited significant corrosion and formation of a thick, porous reaction layer. Although significant corrosion occurred, the specimens were not preferentially attacked along the grain boundaries.

From EPMA quantitative analysis confirmed that the reaction layer on each specimens consisted primarily of $FeGa_3$ with some $CrGa_4$ and Ni_2Ga3. It is possible that ternary and quaternary compounds of iron, chromium, nickel, and gallium also form.

5.2.3 Metal loss

The definition of metal loss is as below:

$$\frac{\Delta t\ (\text{initial base metal} - \text{base metal after exposure})}{2}\ [\mu m]$$

The thickness of initial base metal was measured before exposure to gallium. After testing, specimens was mounted, and sectioned to examination the cross-section of specimens, then the thickness of base metal remaining was measured at six region, and averaged.

Bare metal specimens showed much higher metal loss than other pre-oxidized specimens in gallium environment shown in Figs. 4.20~21. Metal loss decreased in gallium alloy environments as shown in Figs. 4.22~25.

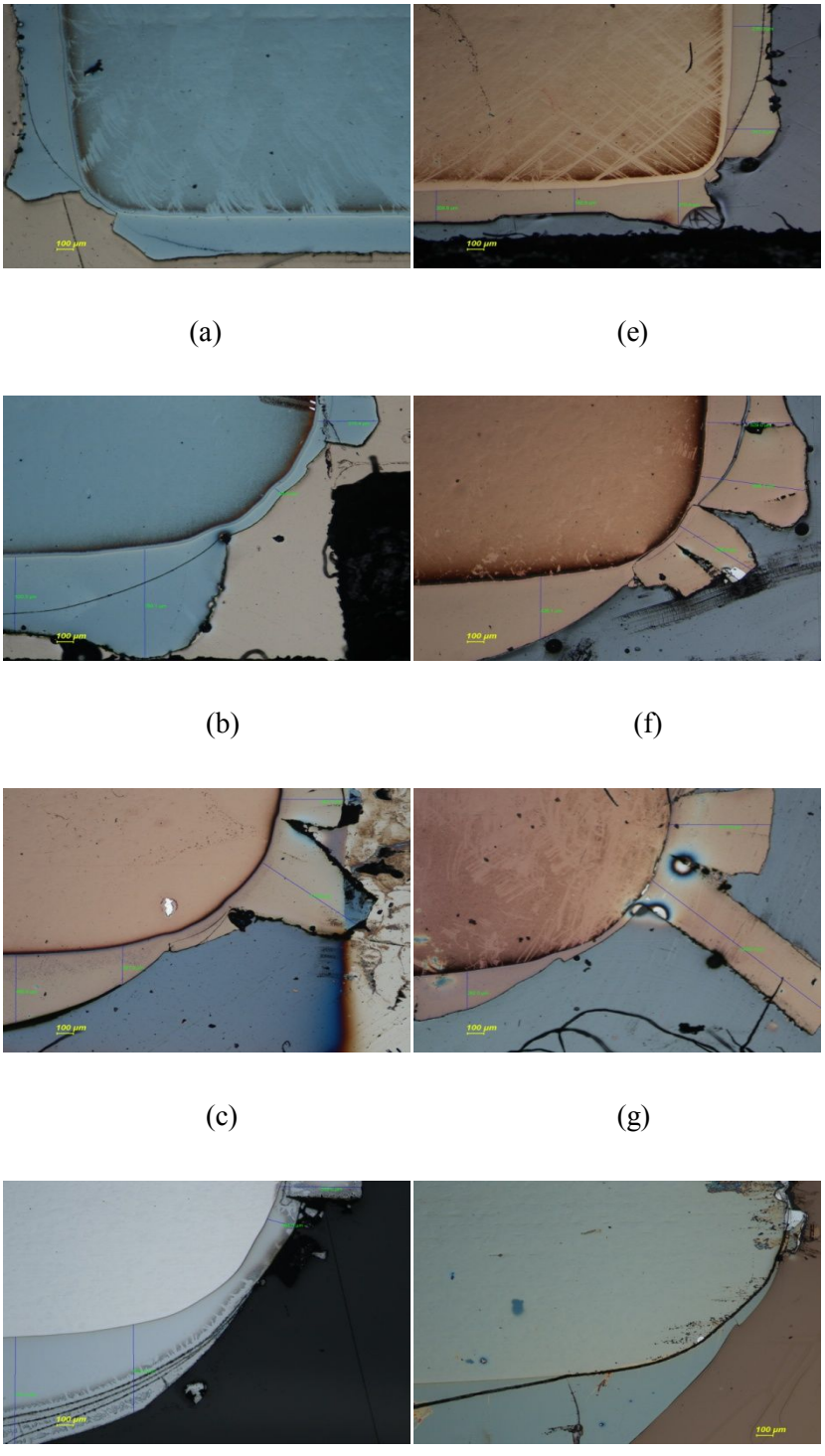

(a) (e)

(b) (f)

(c) (g)

(d) (h)

Fig. 4.1 Optical images of specimens after exposure to static gallium for 17(a), 140(b), 307(c), and 700(d) hr in air condition and 17(e), 140(f), 307(g), and 700(h) hr in vacuum condition, respectively.

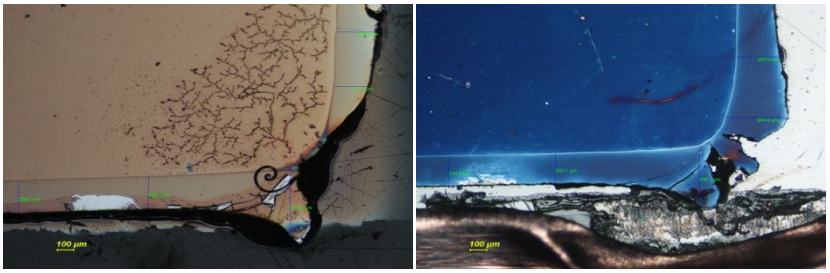

(a) (e)

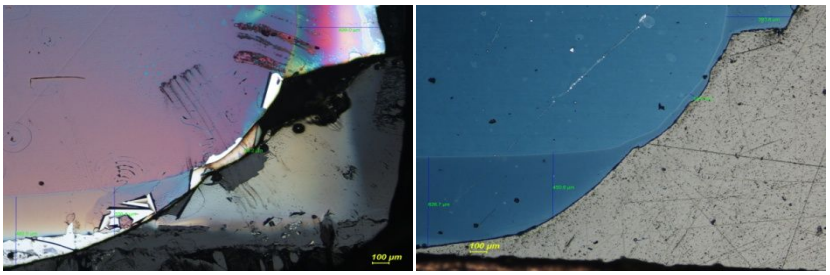

(b) (f)

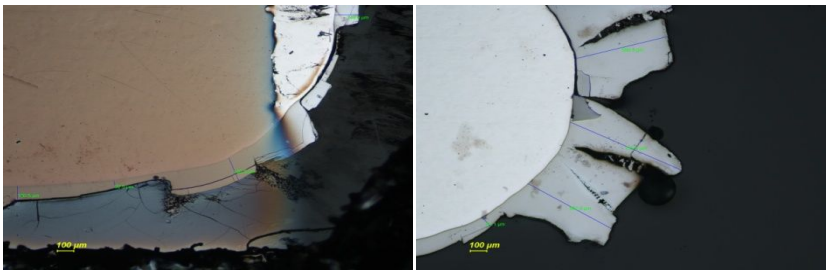

(c) (g)

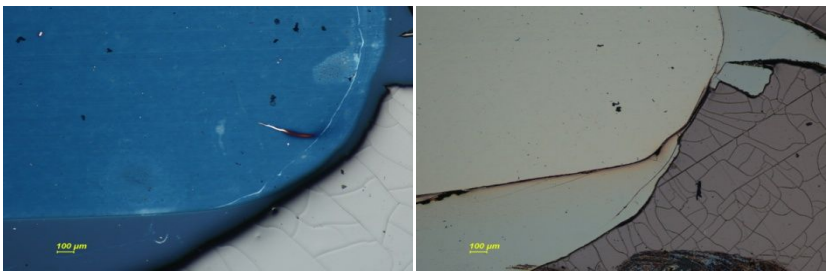

(d) (h)

Fig. 4.2 Optical images of specimens pre-oxidized at 500°C air for 24hr, after exposure to static gallium for 17(a), 140(b), 307(c), and 700(d) hr in air condition and 17(e), 140(f), 307(g), and 700(h) hr in vacuum condition, respectively.

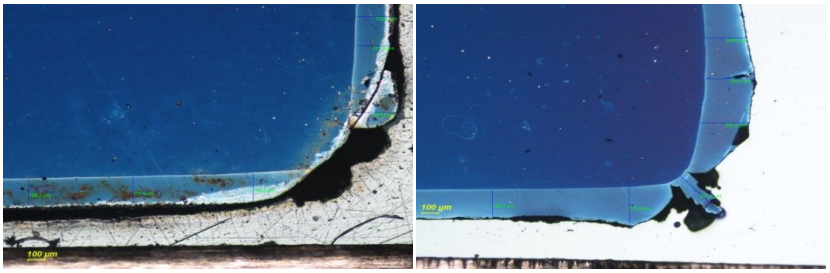

(a) (e)

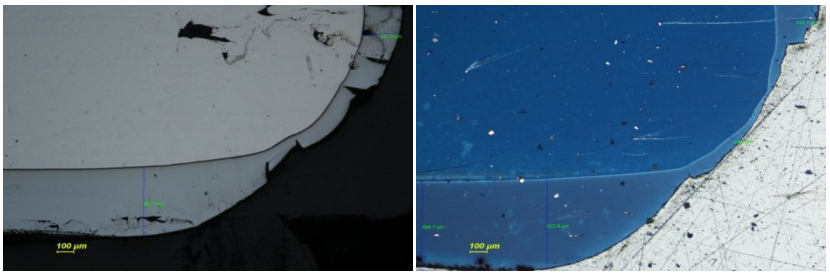

(b) (f)

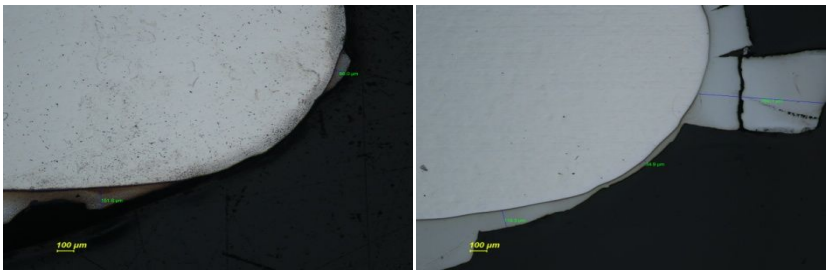

(c) (g)

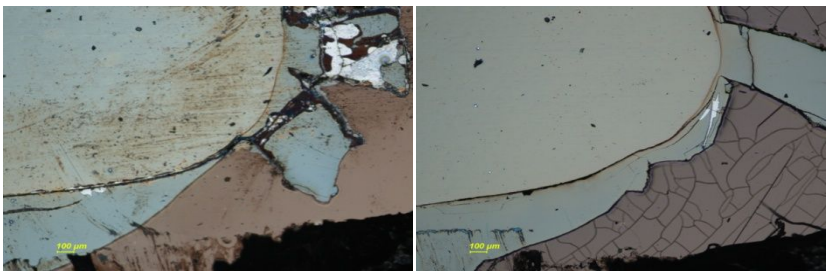

(d) (h)

Fig. 4.3 Optical images of specimens pre-oxidized at 500°C controlled O_2 for 24 hr, after exposure to static gallium for 17(a), 140(b), 307(c), and 700(d) hr in air condition and 17(e), 140(f), 307(g), and 700(h) hr in vacuum condition, respectively.

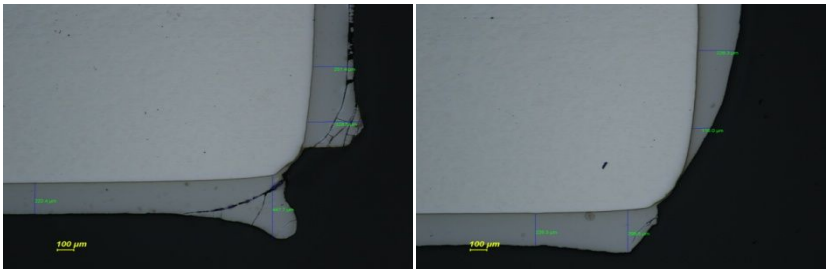

(a) (e)

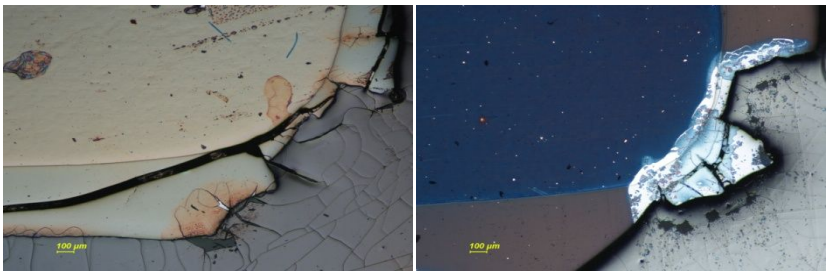

(b) (f)

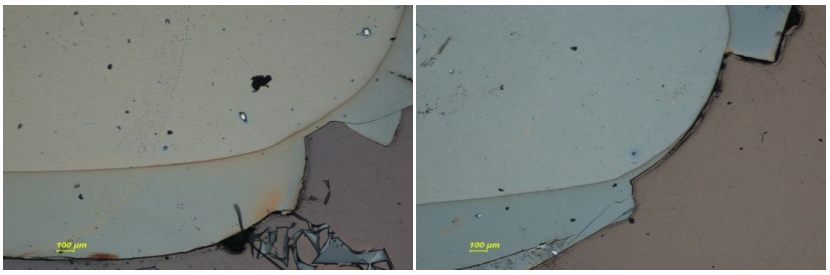

(c) (g)

(d) (h)

Fig. 4.4 Optical images of specimens pre-oxidized at 500°C air for 100hr, after exposure to static gallium for 17(a), 140(b), 307(c), and 700(d) hr in air condition and 17(e), 140(f), 307(g), and 700(h) hr in vacuum condition, respectively.

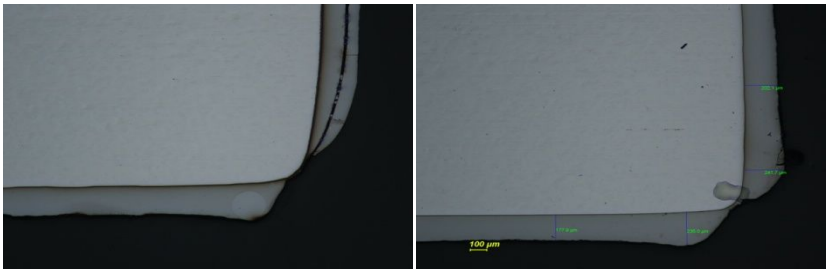

(a) (e)

(b) (f)

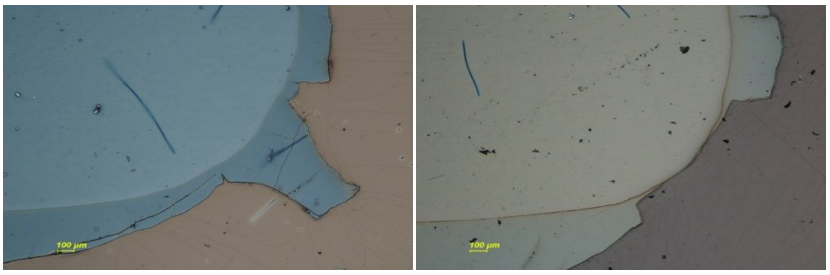

(c) (g)

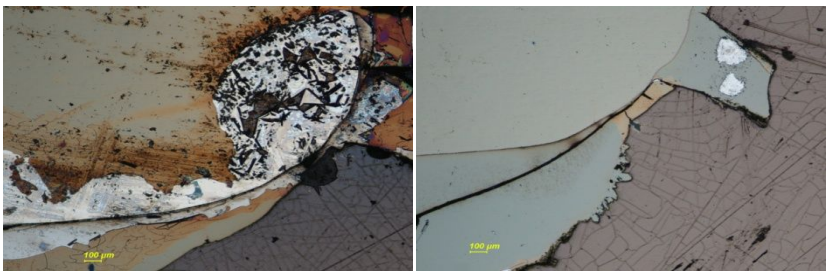

(d) (h)

Fig. 4.5 Optical images of specimens after exposure to gallium alloy (Ga-14Sn-6Zn) for 17(a), 140(b), 307(c), and 700(d) hr in air condition and 17(e), 140(f), 307(g), and 700(h) hr in vacuum condition, respectively.

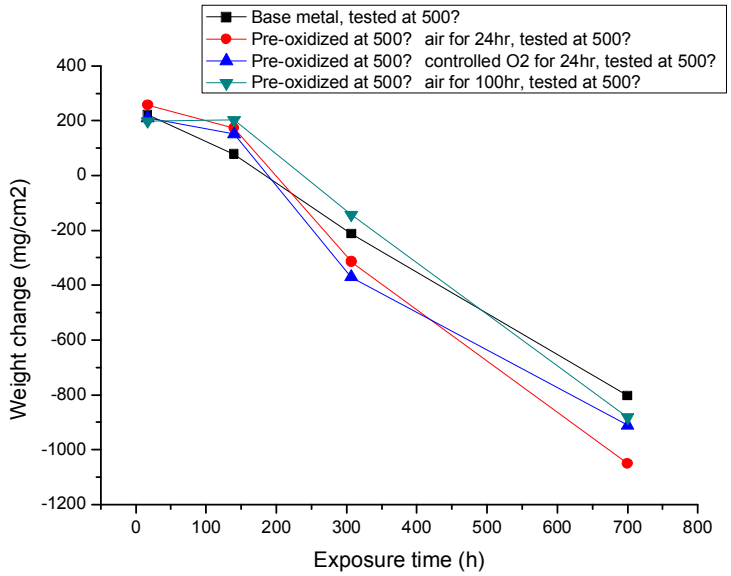

Fig. 4.6 Weight change of vary specimens exposed to static gallium at 500°C, tested in air condition

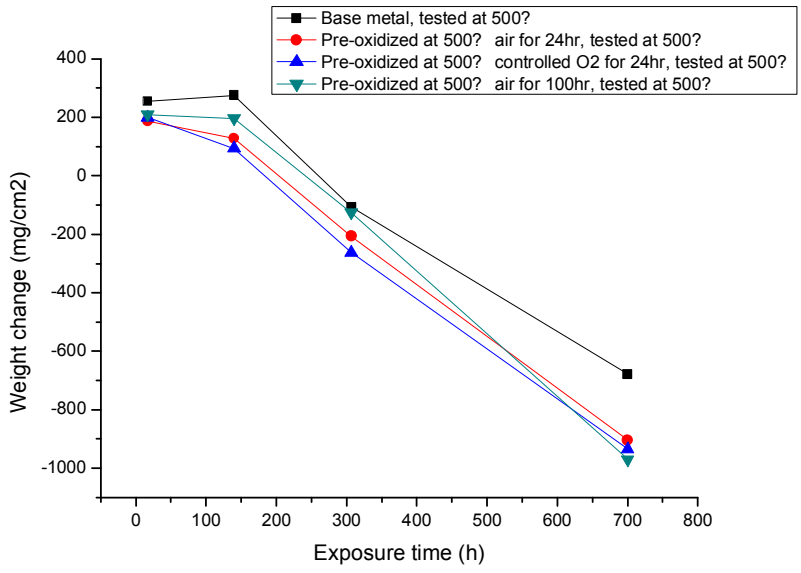

Fig. 4.7 Weight change of vary specimens exposed to static gallium at 500°C, tested in vacuum condition

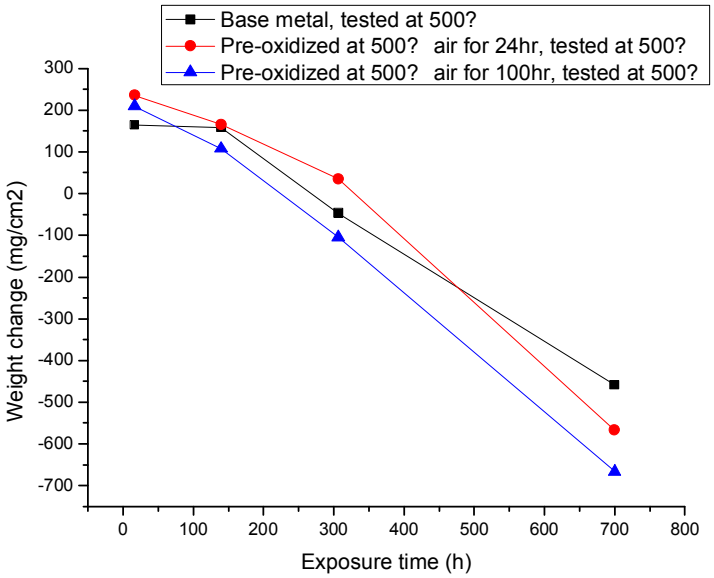

Fig. 4.8 Weight change of vary specimens exposed to gallium alloy (Ga-14Sn-6Zn) at 500°C, tested in air condition

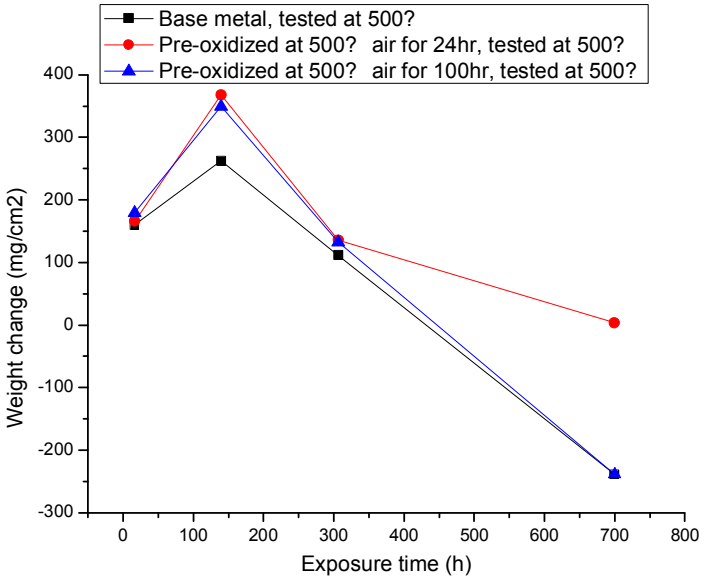

Fig. 4.9 Weight change of vary specimens exposed to gallium alloy (Ga-14Sn-6Zn) at 500°C, tested in vacuum condition

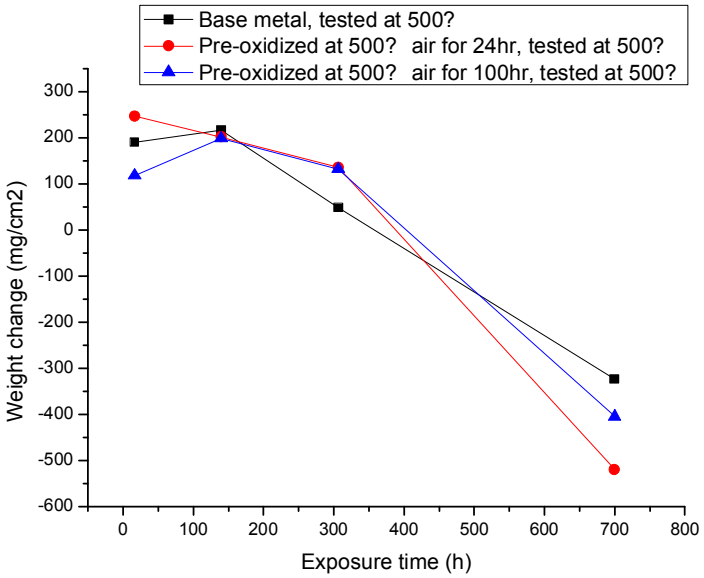

Fig. 4.10 Weight change of vary specimens exposed to gallium alloy (Ga-8Sn-6Zn) at 500°C, tested in air condition

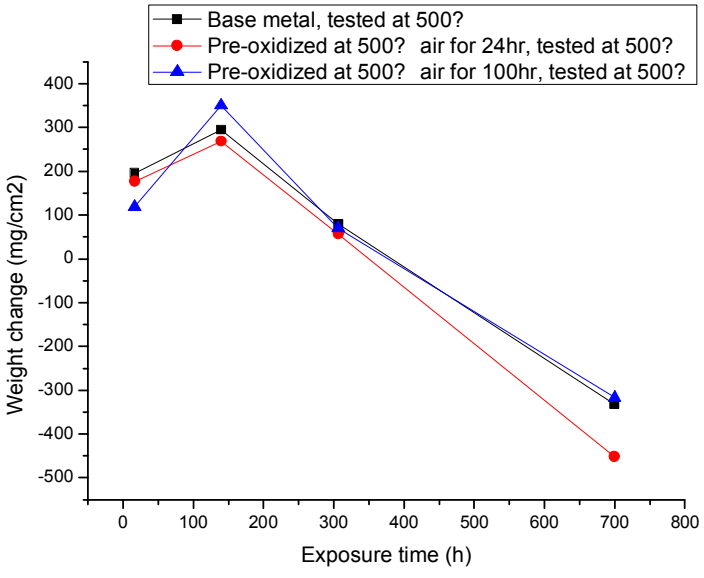

Fig. 4.11 Weight change of vary specimens exposed to gallium alloy (Ga-8Sn-6Zn) at 500°C, tested in vacuum condition

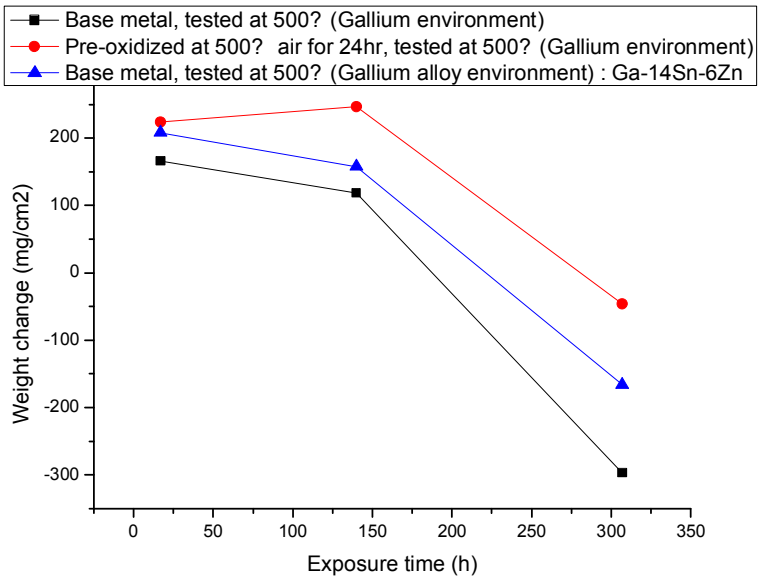

Fig. 4.12 Weight change of vary specimens exposed to gallium and gallium alloy (Ga-14Sn-6Zn) at 500°C, tested in controlled O_2 condition

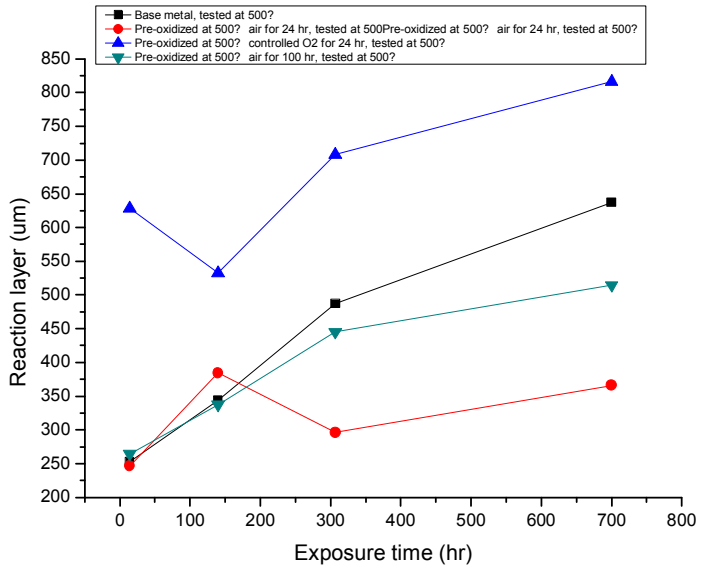

Fig. 4.13 Thickness of reaction layer formed on the surface of specimens in gallium environment tested in air condition

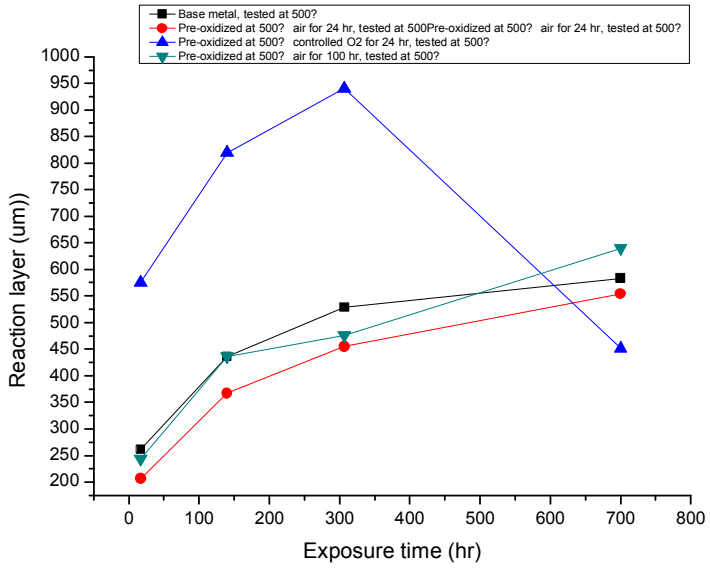

Fig. 4.14 Thickness of reaction layer formed on the surface of specimens in gallium environment tested in vacuum condition

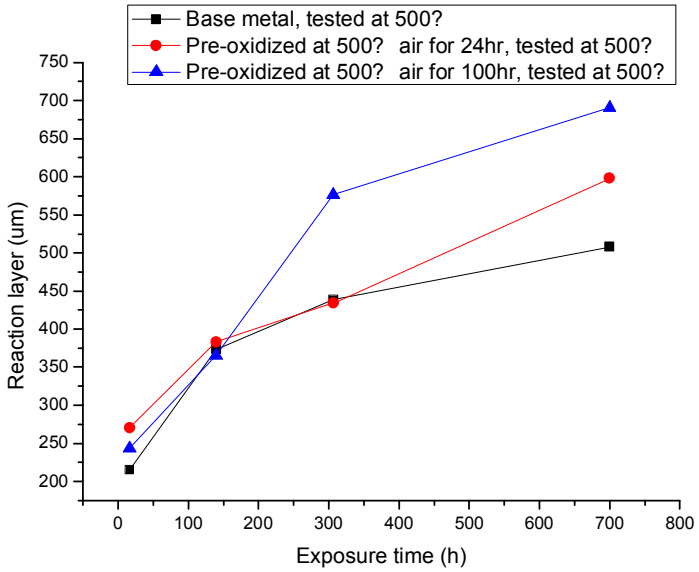

Fig. 4.15 Thickness of reaction layer formed on the surface of specimens in gallium alloy environment (Ga-14Sn-6Zn) tested in air condition

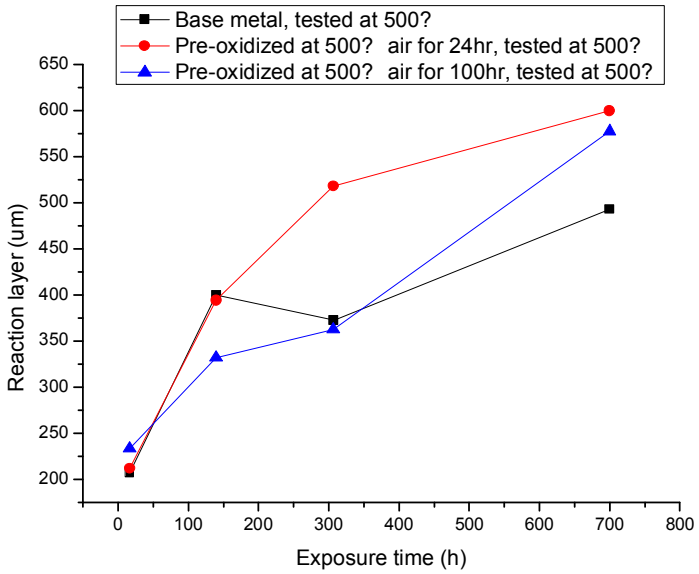

Fig. 4.16 Thickness of reaction layer formed on the surface of specimens in gallium alloy environment (Ga-14Sn-6Zn) tested in vacuum condition

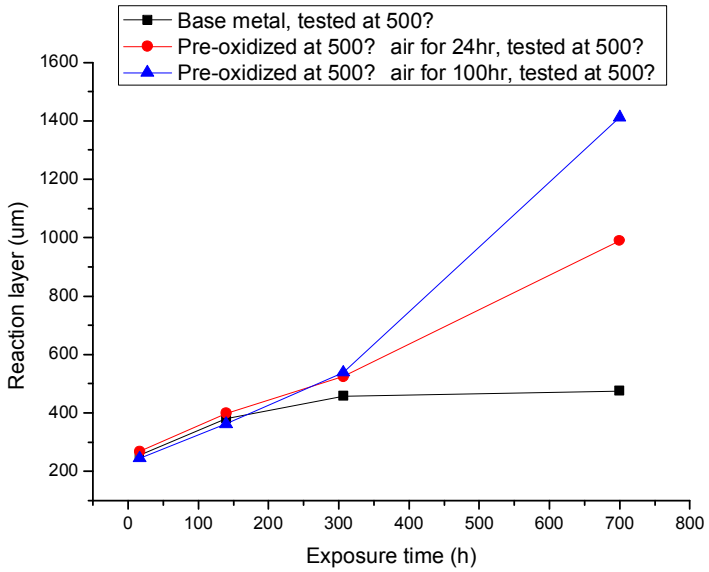

Fig. 4.17 Thickness of reaction layer formed on the surface of specimens in gallium alloy environment (Ga-8Sn-6Zn) tested in air condition

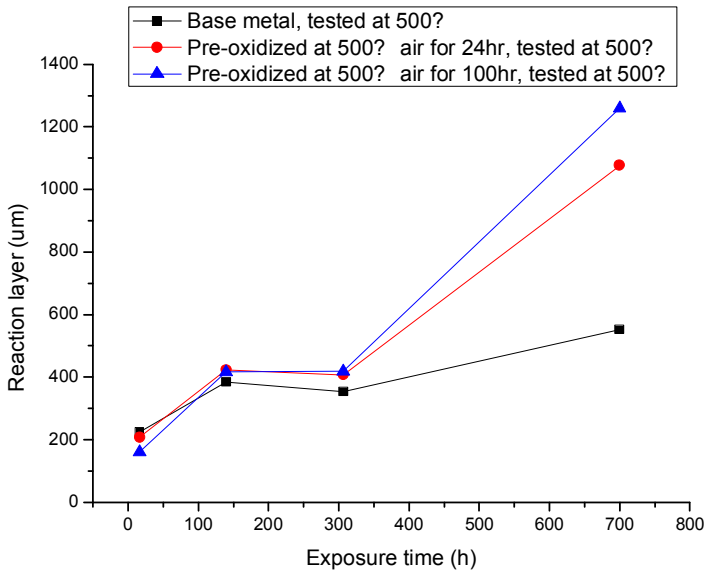

Fig. 4.18 Thickness of reaction layer formed on the surface of specimens in gallium alloy environment (Ga-8Sn-6Zn) tested in vacuum condition

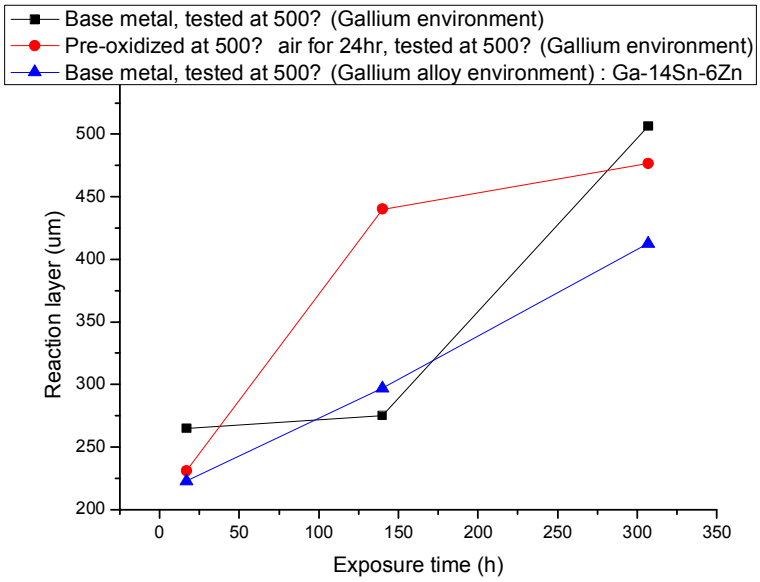

Fig. 4.19 Thickness of reaction layer formed on the surface of specimens in gallium and gallium alloy environment (Ga-14Sn-6Zn) at 500°C, tested in controlled O_2 condition

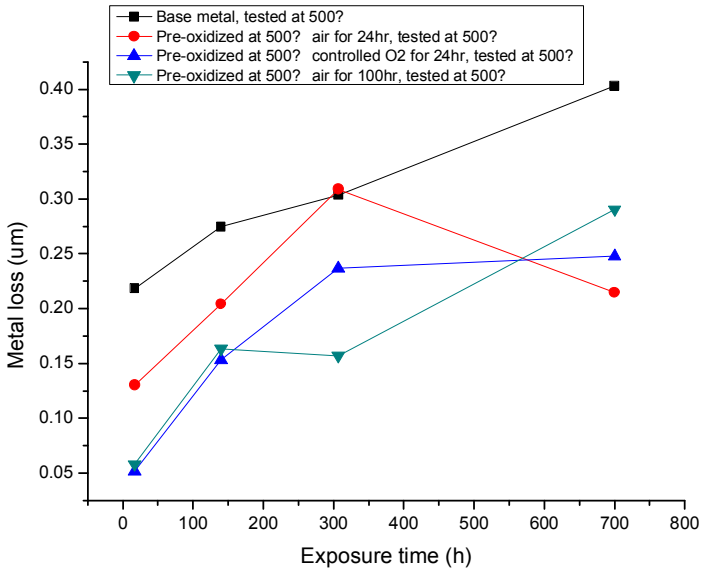

Fig. 4.20 Metal loss of specimens in gallium environment tested in air condition

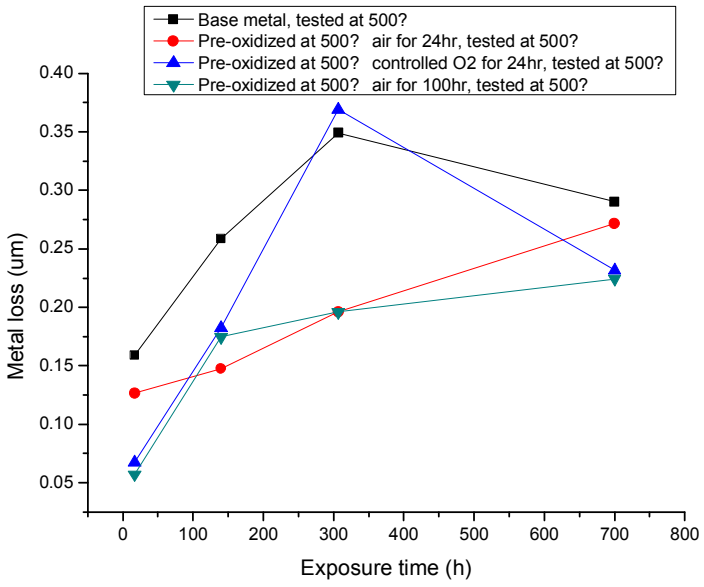

Fig. 4.21 Metal loss of specimens in gallium environment tested in vacuum condition

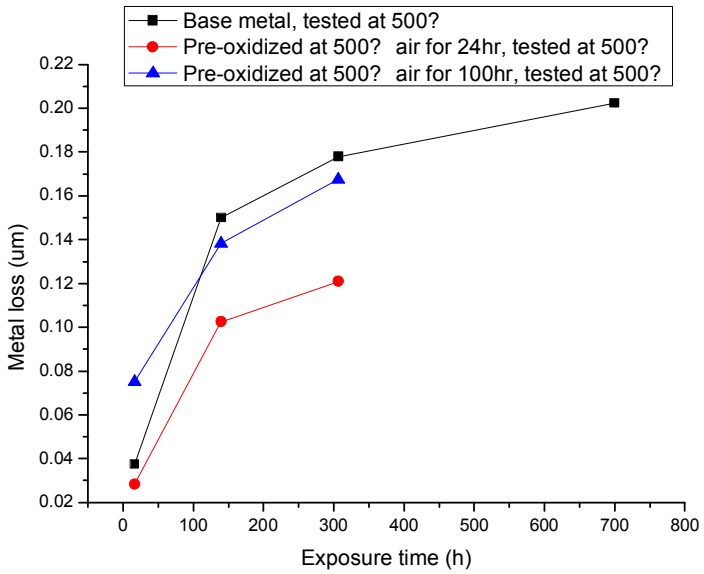

Fig. 4.22 Metal loss of specimens in gallium alloy environment (Ga-14Sn-6Zn) tested in air condition

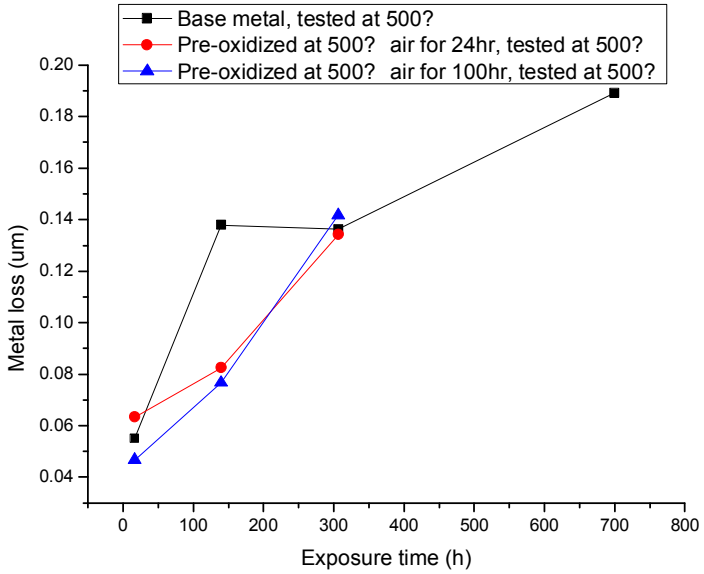

Fig. 4.23 Metal loss of specimens in gallium alloy environment (Ga-14Sn-6Zn) tested in vacuum condition

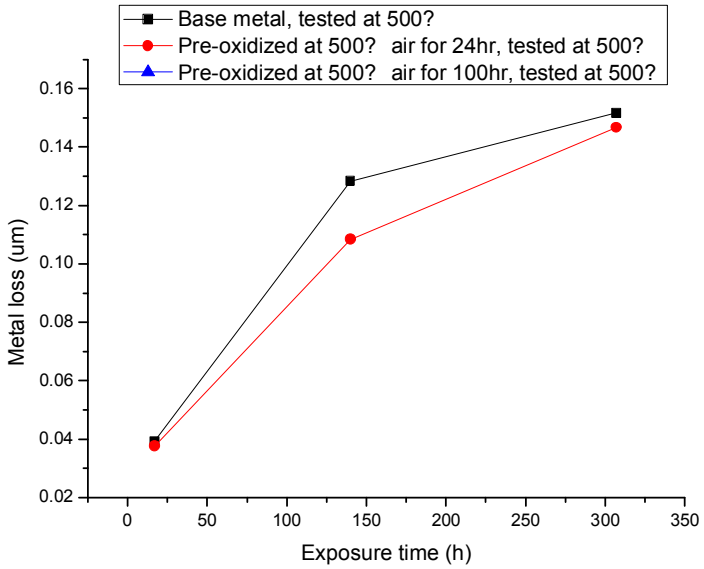

Fig. 4.24 Metal loss of specimens in gallium alloy environment (Ga-8Sn-6Zn) tested in air condition

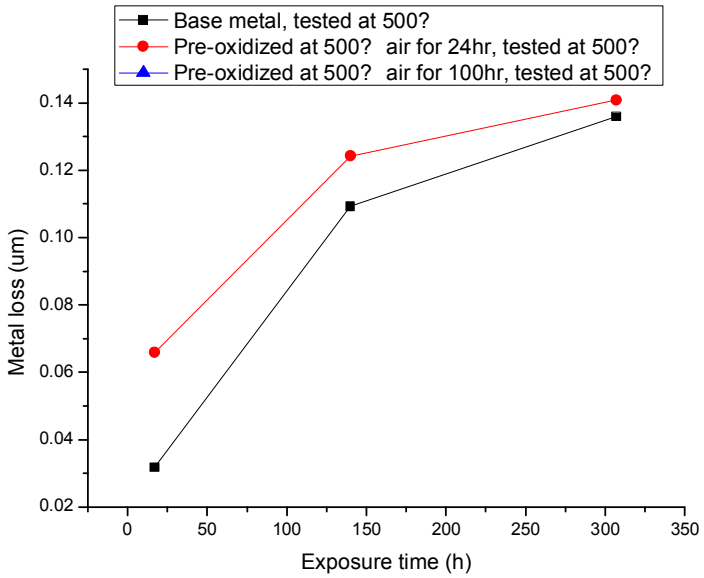

Fig. 4.25 Metal loss of specimens in gallium alloy environment (Ga-8Sn-6Zn) tested in vacuum condition

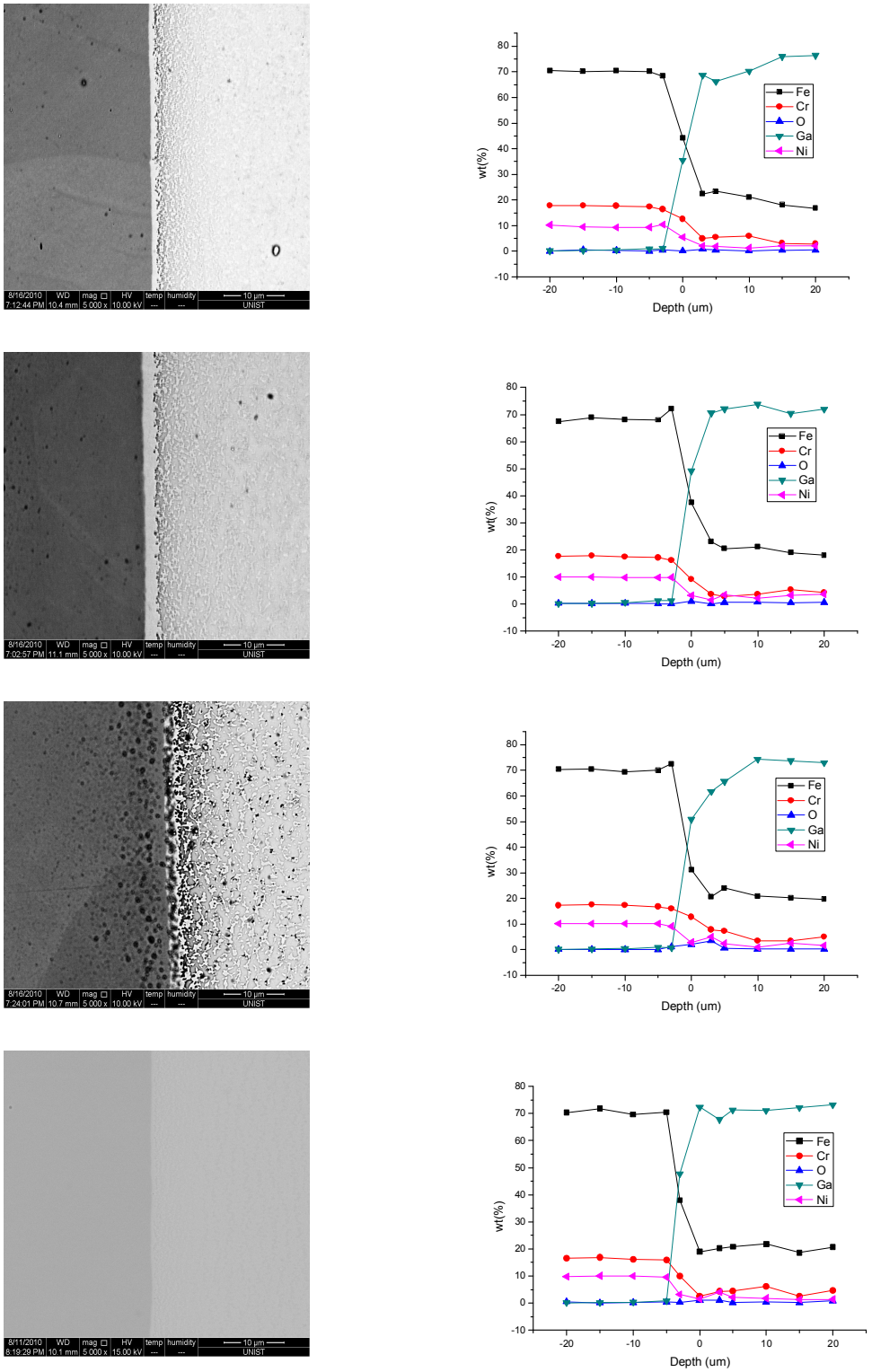

Fig. 4.26 SEM Images of SS 316L after exposure to static gallium at 500°C in air for 17, 140, 307, and 700 hrs, along red (steel region) and blue (gallium compound region) spots indicating analysis positions for EPMA (left) and quantitative analysis of Fe, Cr, O, Ga, and Ni obtained by EPMA (right).

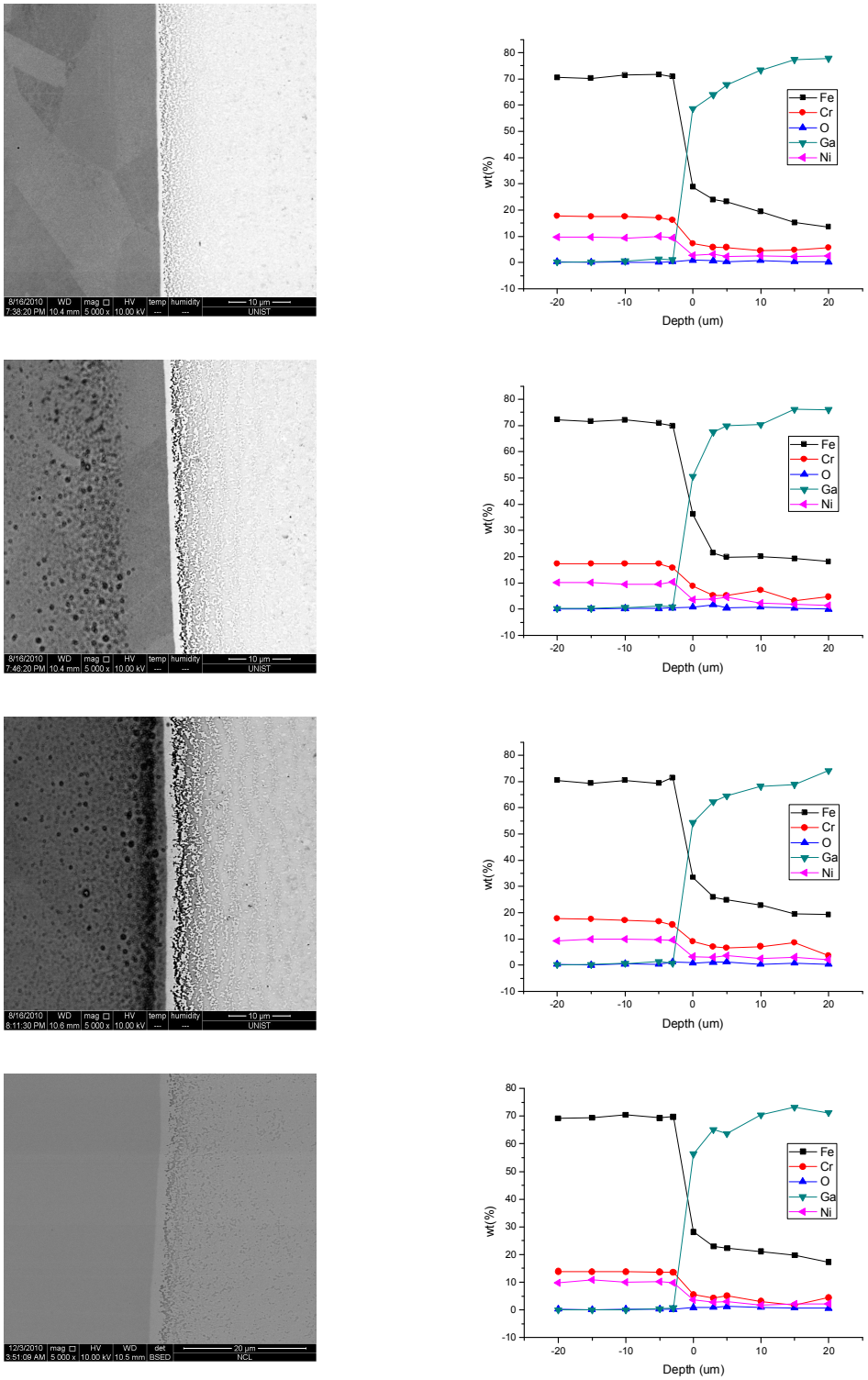

Fig. 4.27 SEM Images of SS 316L after exposure to static gallium at 500°C in vacuum for 17, 140, 307, and 700 hrs, along red (steel region) and blue (gallium compound region) spots indicating analysis positions for EPMA (left) and quantitative analysis of Fe, Cr, O, Ga, and Ni obtained by EPMA (right).

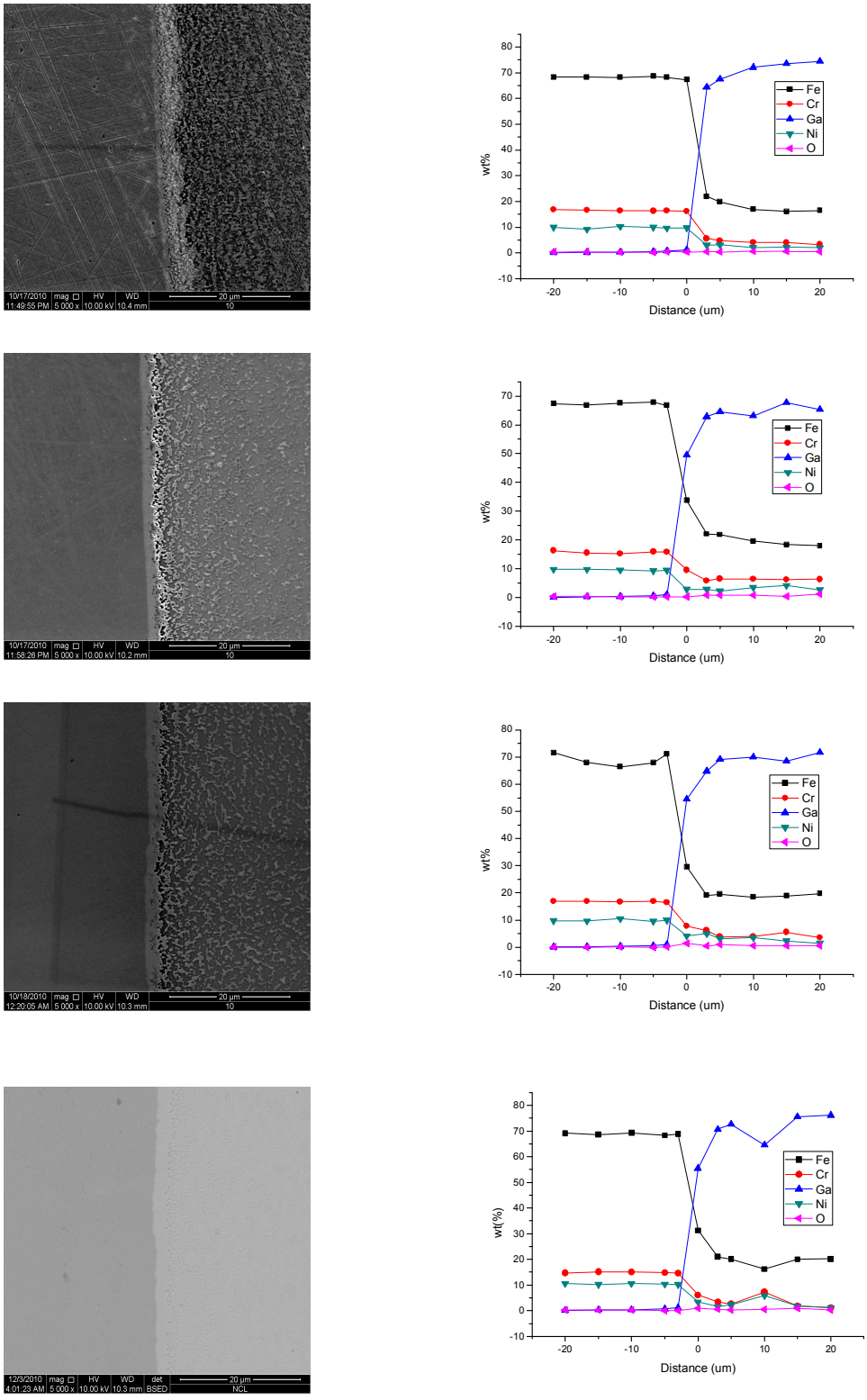

Fig. 4.28 SEM Images of pre-oxidized SS 316L at 500°C air for 24hr, after exposure to static gallium at 500°C in air for 17, 140, 307, and 700 hrs, along red (steel region) and blue (gallium compound region) spots indicating analysis positions for EPMA (left) and quantitative analysis of Fe, Cr, O, Ga, and Ni obtained by EPMA (right).

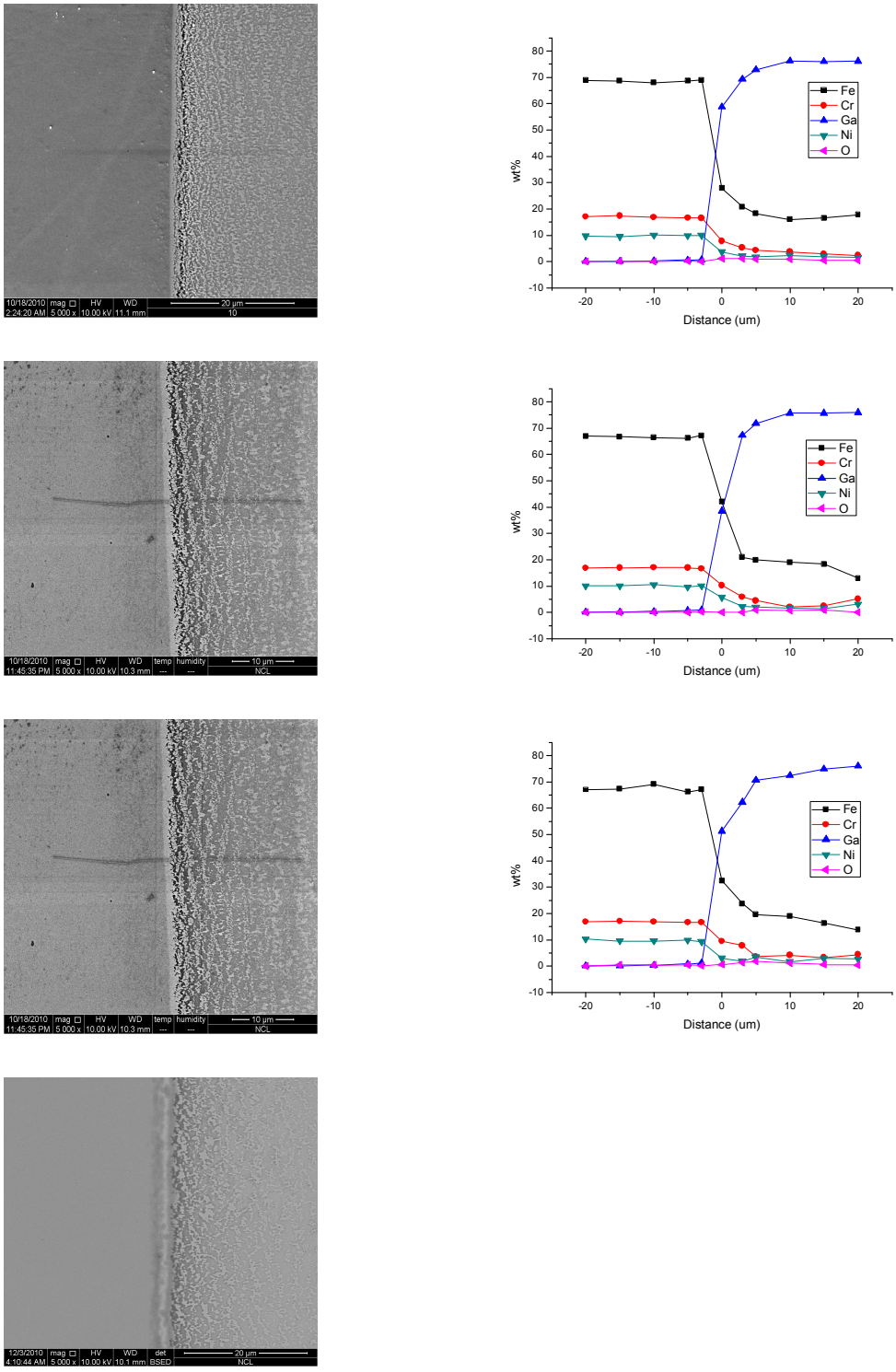

Fig. 4.29 SEM Images of pre-oxidized SS 316L at 500°C air for 24hr, after exposure to static gallium at 500°C in vacuum for 17, 140, 307, and 700 hrs, along red (steel region) and blue (gallium compound region) spots indicating analysis positions for EPMA (left) and quantitative analysis of Fe, Cr, O, Ga, and Ni obtained by EPMA (right).

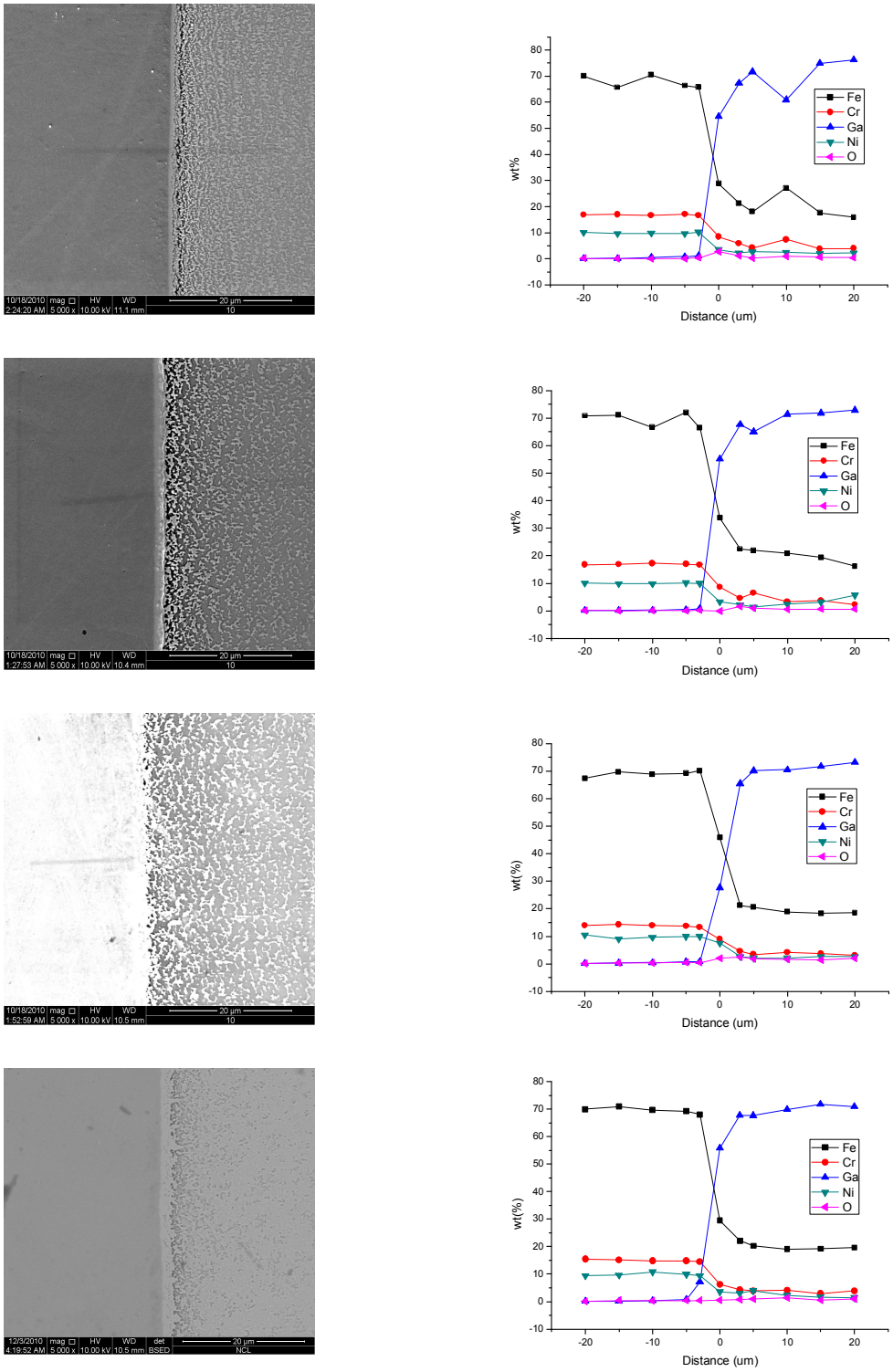

Fig. 4.30 SEM Images of pre-oxidized SS 316L at 500°C controlled O_2 for 24hr, after exposure to static gallium at 500°C in air for 17, 140, 307, and 700 hrs, along red (steel region) and blue (gallium compound region) spots indicating analysis positions for EPMA (left) and quantitative analysis of Fe, Cr, O, Ga, and Ni obtained by EPMA (right).

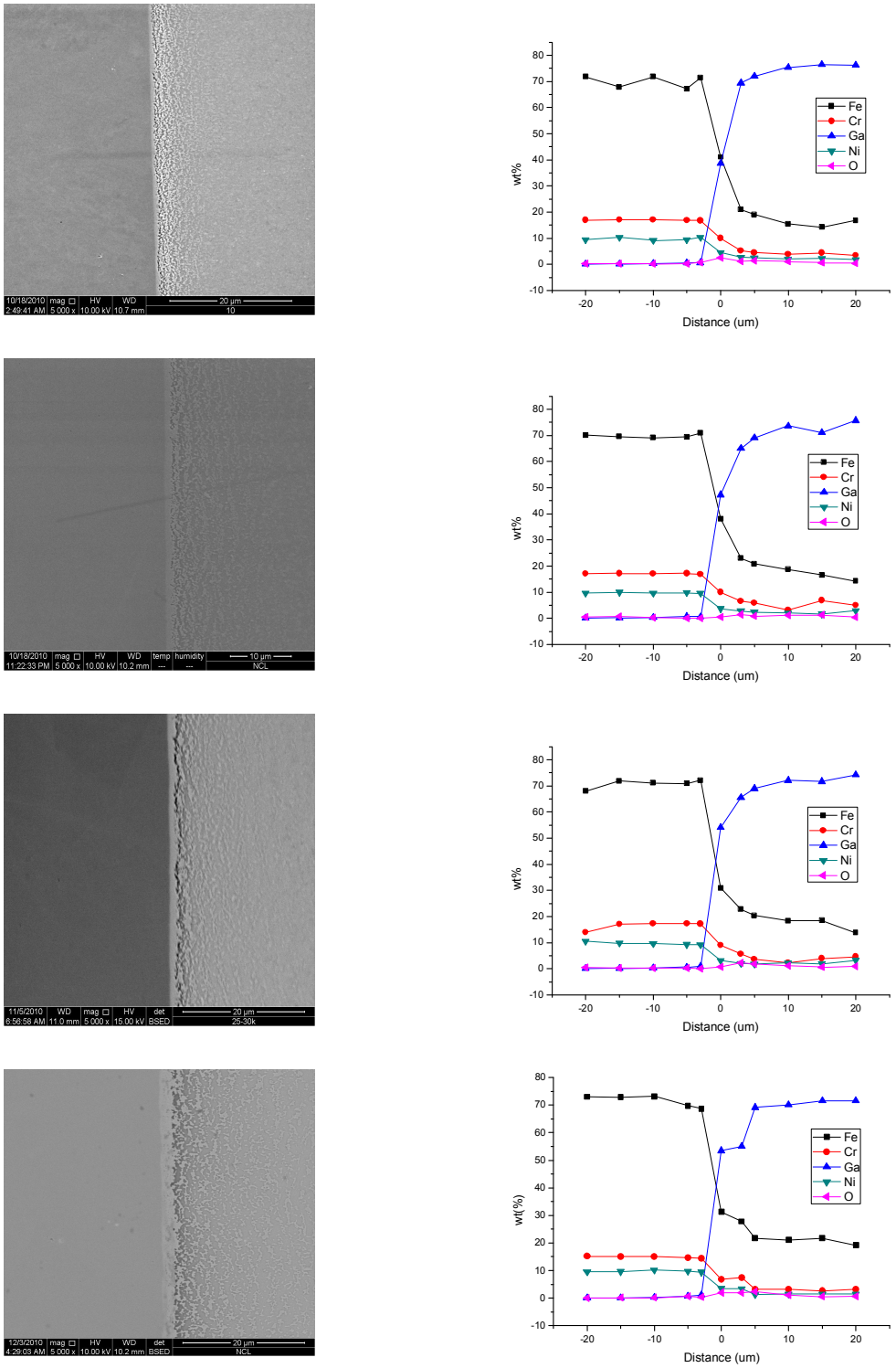

Fig. 4.31 SEM Images of pre-oxidized SS 316L at 500°C controlled O_2 for 24hr, after exposure to static gallium at 500°C in vacuum for 17, 140, 307, and 700 hrs, along red (steel region) and blue (gallium compound region) spots indicating analysis positions for EPMA (left) and quantitative analysis of Fe, Cr, O, Ga, and Ni obtained by EPMA (right).

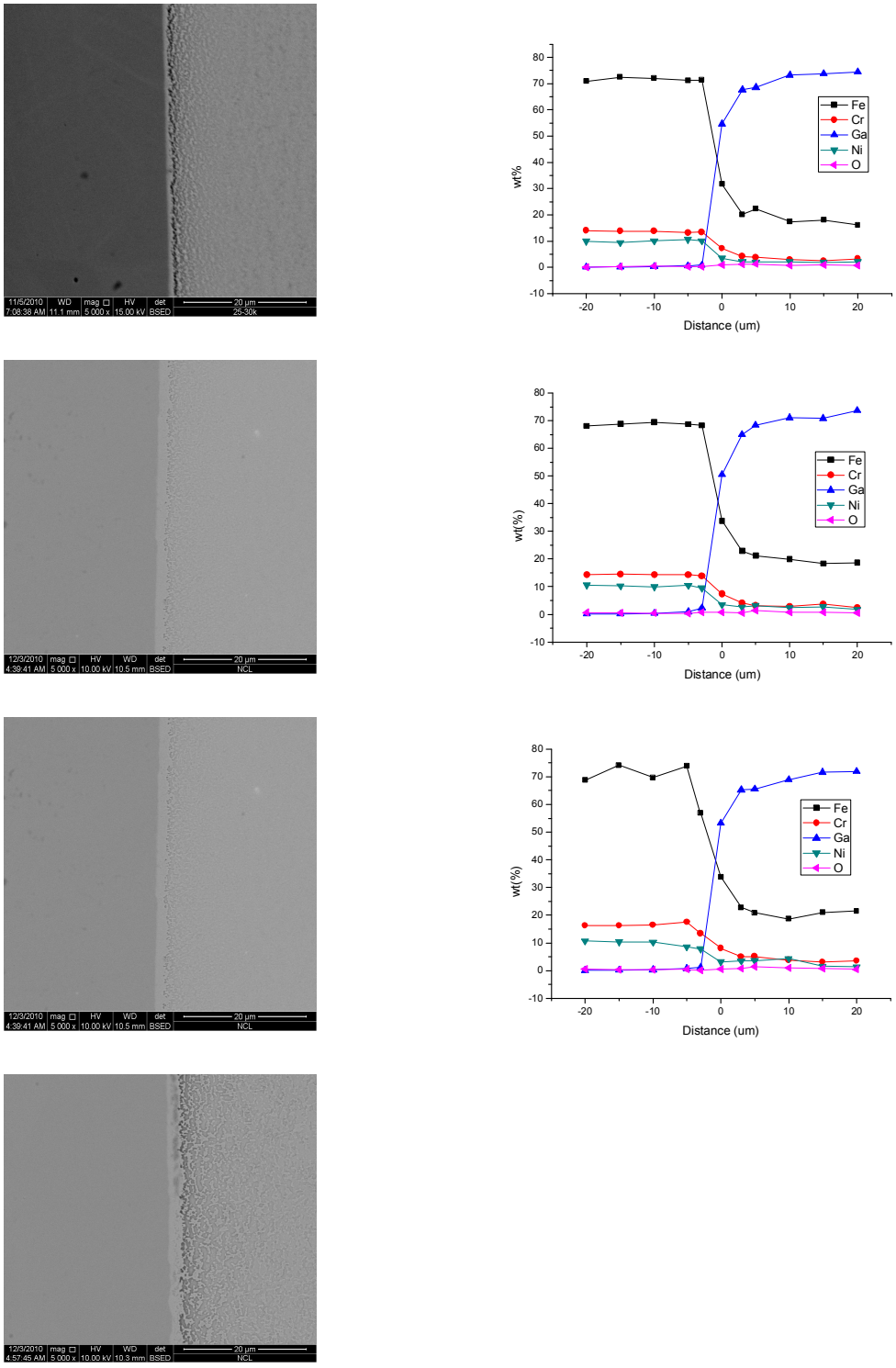

Fig. 4.32 SEM Images of pre-oxidized SS 316L at 500°C air for 100hr, after exposure to static gallium at 500°C in air for 17, 140, 307, and 700 hrs, along red (steel region) and blue (gallium compound region) spots indicating analysis positions for EPMA (left) and quantitative analysis of Fe, Cr, O, Ga, and Ni obtained by EPMA (right).

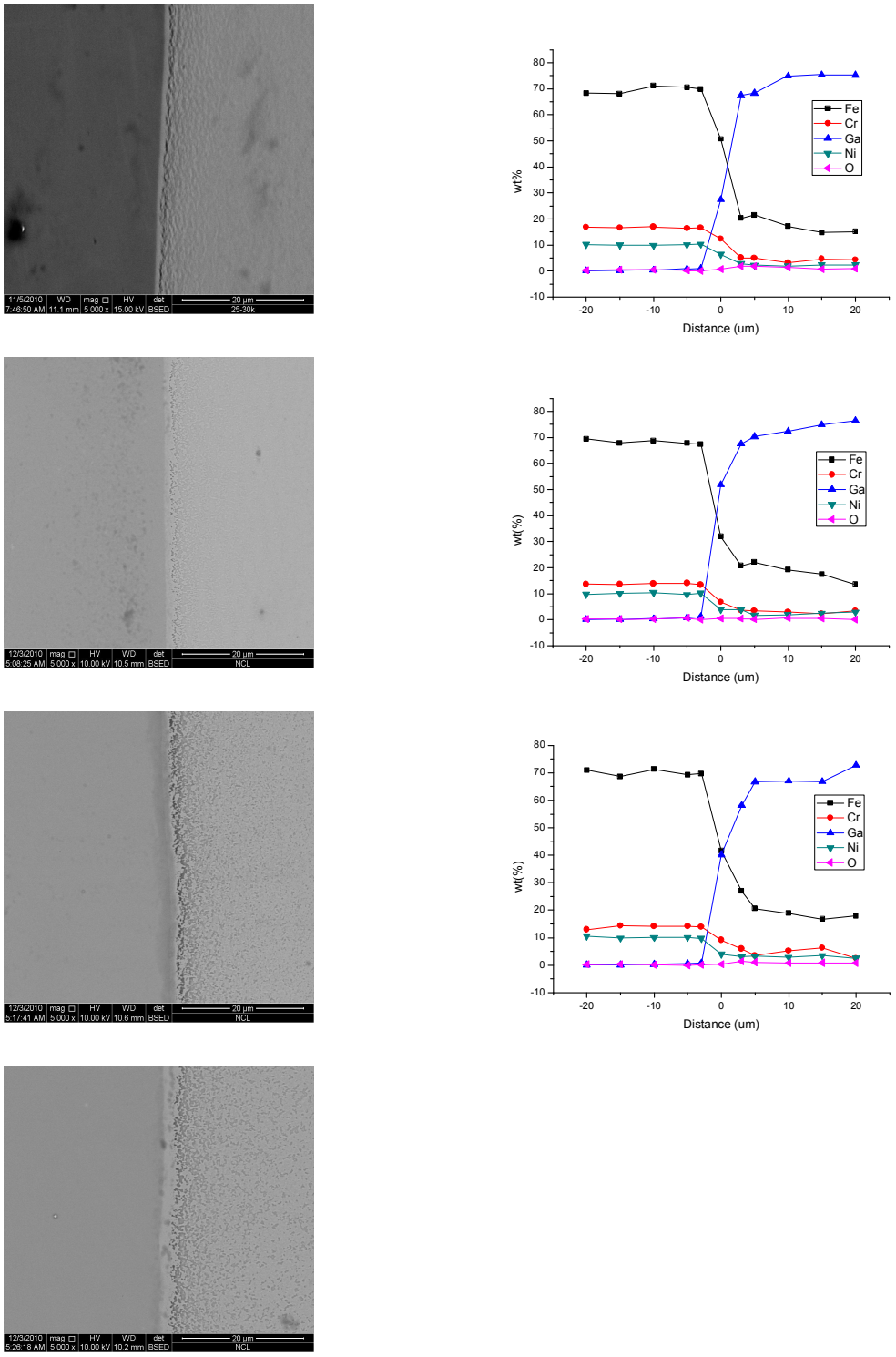

Fig. 4.33 SEM Images of pre-oxidized SS 316L at 500°C air for 100hr, after exposure to static gallium at 500°C in vacuum for 17, 140, 307, and 700 hrs, along red (steel region) and blue (gallium compound region) spots indicating analysis positions for EPMA (left) and quantitative analysis of Fe, Cr, O, Ga, and Ni obtained by EPMA (right).

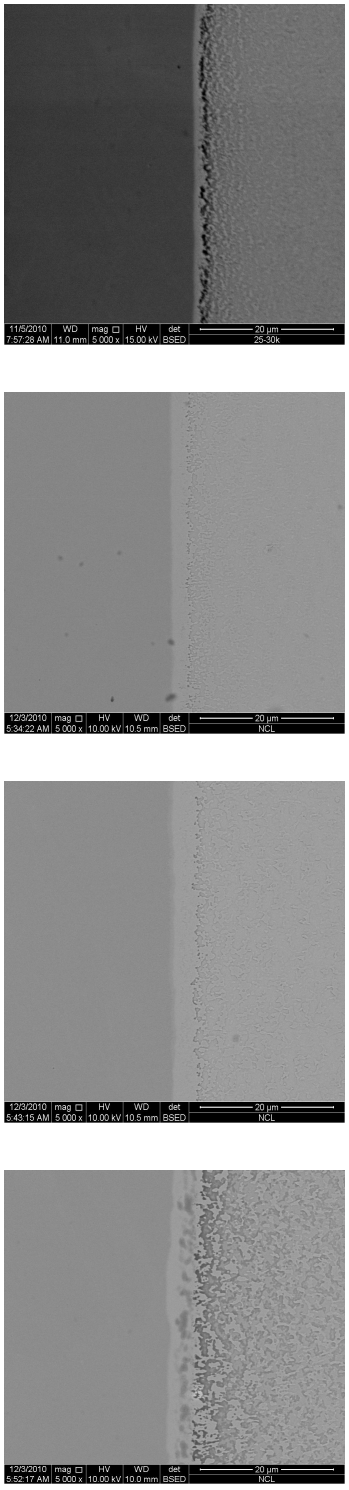

Fig. 4.34 SEM Images of SS 316L after exposure to static gallium alloy (Ga-14Sn-6Zn) at 500°C in air for 17, 140, 307, and 700 hrs, along red (steel region) and blue (gallium compound region) spots indicating analysis positions for EPMA (left) and quantitative analysis of Fe, Cr, O, Ga, Ni, Sn and Zn obtained by EPMA (right).

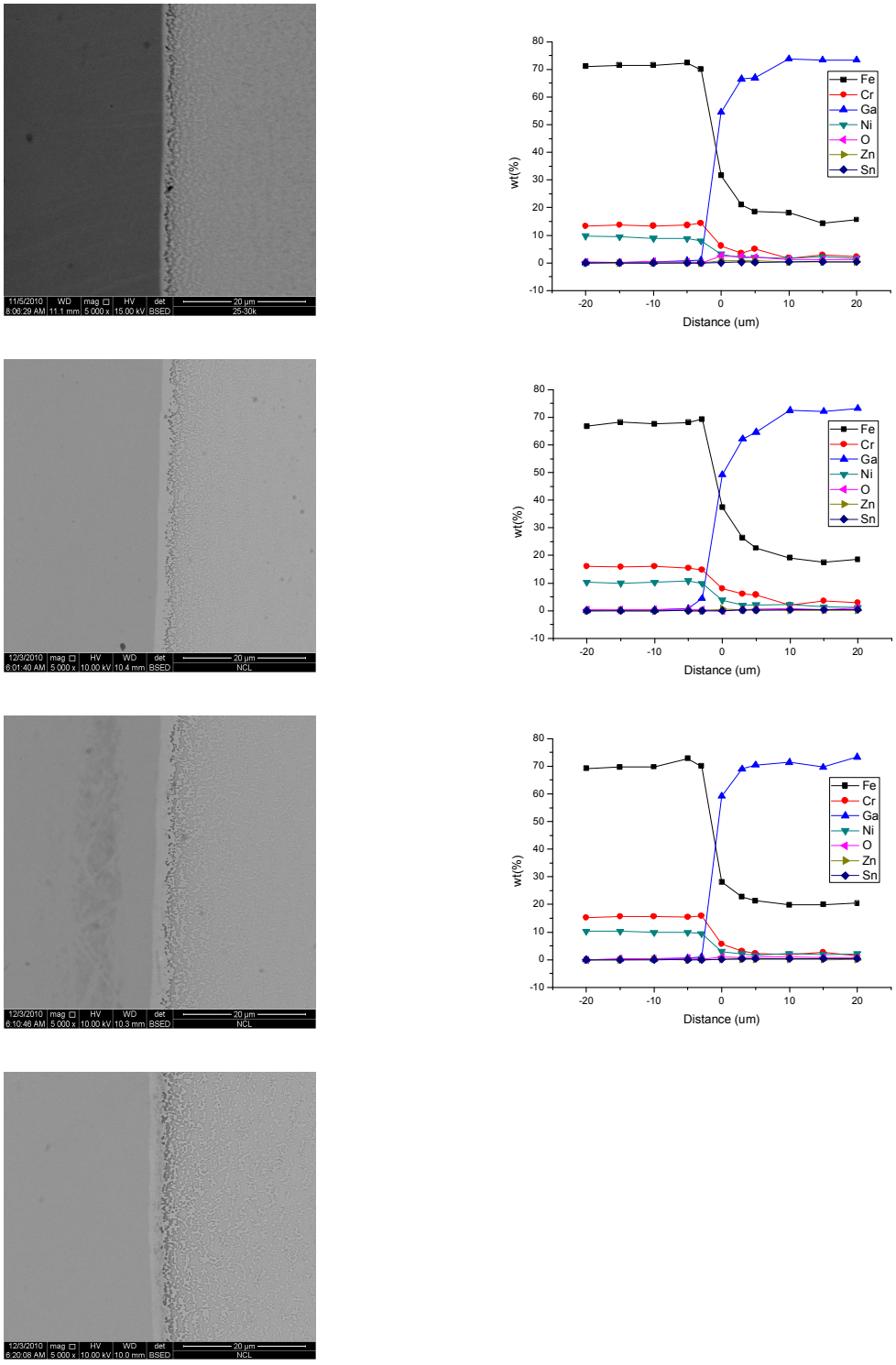

Fig. 4.35 SEM Images of SS 316L after exposure to static gallium alloy (Ga-14Sn-6Zn) at 500°C in vacuum for 17, 140, 307, and 700 hrs, along red (steel region) and blue (gallium compound region) spots indicating analysis positions for EPMA (left) and quantitative analysis of Fe, Cr, O, Ga, Ni, Sn and Zn obtained by EPMA (right).

REFERENCES

1. Luebbers, PR 1993, ‘Compatibility of ITER candidate structural materials with static gallium’, Argonne National Laboratory, U.S DOE

2. Yatsenko, SP 1970, ‘Solubility of metals of fifth period in liquid gallium’, Sov. Mater. Sci., Vol. 6

3. Prokhorenko V 2000, ‘Liquid gallium: potential uses as a heat-transfer agent’, High temperature, Vol. 38,

VI. Discussion

6.1 Phase of reaction layer

Depending on EPMA quantitative analysis, the reaction layers on the specimens tested in gallium environment are mainly consisted of gallium, iron, chromium, and nickel. The possible phases in reaction layer are mainly FeGa3 with some CrGa4 and Ni2Ga3 [1, 2, 3, 4]. It is possible that ternary and quaternary compounds also formed.

The reaction layers of specimens exposed to gallium alloy environments (both Ga-14Sn-6Zn and Ga-8Sn-6Zn) also consisted of gallium, iron, chromium, and nickel with 1~2 wt% of zinc only near the interface. The amount of tin in gallium alloys is higher than that of zinc. Tin was not observed in reaction layer. Depending on the phase diagrams of Ga-Sn [6] and Ga-Zn [7], gallium is not compoundable with tin and zinc as shown in Figs. 6.1 and 6.2. But iron can be compounded with zinc as shown Fig. 6.3. So, it is possible that zinc was compounded with iron.

6.2 Effect of gallium alloy on corrosion behavior of structural materials

In this thesis work, all specimens were exposed to three conditions of environments as below:

1) gallium environment

2) Ga-14Sn-6Zn environment

3) Ga-8Sn-6Zn environment

Depending on corrosion behavior data, the weight change of bare specimens exposed to gallium was -804.32 mg/cm^2 (in air condition) and -678.7 mg/cm^2 (in vacuum condition), respectively. At Ga-14Sn-6Zn environment, the values are -458.9 mg/cm^2 (in air condition) and -238.9 mg/cm^2 (in vacuum condition) and at Ga-8Sn-6Zn, the values are -324 mg/cm^2 (in air condition) and -316.7 mg/cm^2 (in vacuum condition), respectively. The weight change of bare specimens that exposed to gallium alloys is smaller than that exposed to gallium.

The thickness of reaction layer is not affected by these environments. Specimens that exposed to gallium alloys have 1~2 wt% of zinc in the reaction layer neat the interface.

Metal loss of bare specimens that exposed to gallium is 0.4029μm (in air condition) and 0.29μm (in vacuum condition). In Ga-14Sn-6Zn environment, the values are reduced as 0.2025μm (in air condition) and 0.1892μm (in vacuum condition). The expected metal loss in Ga-8Sn-6Zn environment is the values between gallium and Ga-14Sn-6Zn, but the values are again reduced such as 0.1517μm (in air condition) and 0.1358μm (in vacuum condition).

6.3 Effect of oxide layer on corrosion behavior of structural materials

In this thesis, specimens were pre-oxidized under three conditions as below:

1) pre-oxidized at 500°C air for 24 hr

2) pre-oxidized at 500°C air for 100 hr

3) pre-oxidized at 500°C controlled O_2 for 24 hr

The pre-oxidized specimens that exposed to gallium and Ga-8Sn-6Zn environments gained their weight more than that of bare specimens. Pre-oxidized specimens that exposed to Ga-14Sn-6Zn environment gained more in air condition and lost more in vacuum conditions compared to bare specimens as shown in Figs. 4.8~9.

About the thickness of reaction layer, especially specimens that pre-oxidized at 500°C controlled O_2 for 24 hr developed 816.7μm (in air condition) and 451.3μm (in vacuum condition), respectively. For times up to 307 hr, the thickness of reaction layer of these specimens was thick twice in both air and vacuum conditions. In air condition, this tendency was kept until times up to 700 hr, however the specimen tested in vacuum condition for 700 hr did not show this tendency as shown in Figs. 4.13 and 14. General behavior of developing reaction layer within the effect of pre-oxidation is that pre-oxidized specimens, in any conditions, had developed as thick as reaction layers on bare specimens.

In Figs. 4.20 and 21, the metal loss of bare specimens were 0.4029μm (in air condition) and 0.29μm (in vacuum condition), respectively. But metal loss of other pre-oxidized specimens was reduced due to pre-oxidation process as shown in Figs. 4. 20 and 21.

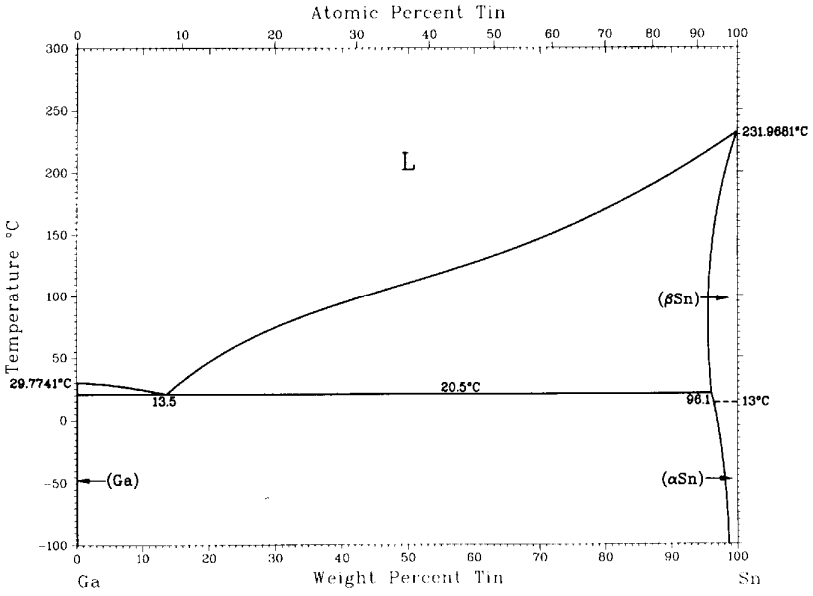

Fig. 6.1 The phase diagram of Ga-Sn system [6]

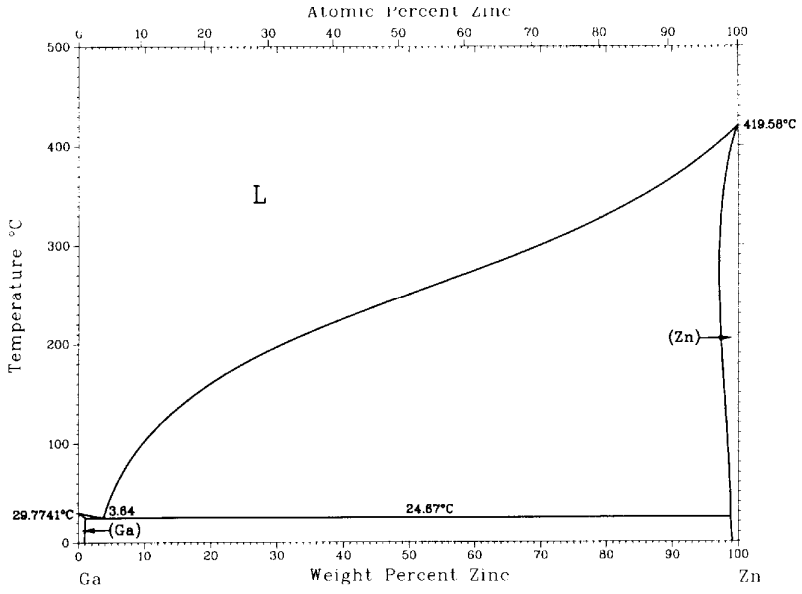

Fig. 6.2 The phase diagram of Ga-Zn system [7]

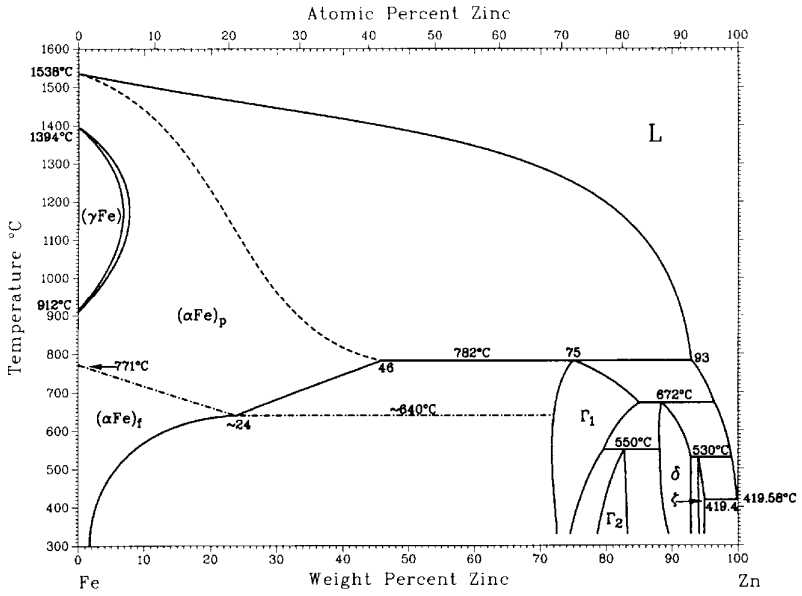

Fig. 6.3 The phase diagram of Fe-Zn system [8]

REFERENCES

1. Luebbers, P. R., Michaud, W. F. & Chopra, O. K 1993, Compatibility of ITER Candidate Structural Materials with Static Gallium, *Argonne National Laboratory ANL-93/31*

2. Okamoto, H 2004, Fe-Ga (Iron-Gallium), *Journal of Phase Equilibria and Diffusion,* vol. 25, 100

3. Okamoto, H 2007, Cr-Ga (Chromium-Gallium), *Journal of Phase Equilibria and Diffusion,* vol. 28, 301

4. Okamoto, H 2008, Ga-Ni (Gallium-Nickel), *Journal of Phase Equilibria and Diffusion,* vol. 29, 296

5. Old, C. F 1980, Liquid metal Embrittlement of nuclear materials, *Journal of nuclear materials,* vol. 92, 2-25

6. Anderson, T. J & Ansara, I 1992, 'The Ga-Sn (gallium-tin) system', *Journal of Phase Equilabria,* vol. 13, 181-189

7. Dutkiewicz, J., Moser, Z., Zabdyr, L., Gohil, D. D., Chart, T. G., Ansara, I., & Girard, C 1990, 'The Ga-Zn (Gallium-Zinc) system, *Journal of Phase Equilabria,* vol. 11, 77-82

8. Burton, B. P 1993, 'Phase diagram of binary iron alloys', *American Society for Metals,* Chapters on Al-Fe, Fe-K, Fe-Na, Fe-Pb, Fe-Rb, and Fe-Zn.

VII. Summary and conclusion

After bare specimens exposed to liquid gallium at 500°C, the volume of specimens which tested in air and vacuum condition was significantly reduced. It is due to dissolution of constituents of solid metal into liquid gallium.

Pre-oxidation of SS 316L under three conditions in this study shows difference of corrosion behavior, but is not effective to prevent the mass transfer of constituents of the steels, even under actively controlled O_2 condition. The weight change and metal loss are generally reduced in vacuum condition and also in gallium alloy environments, but still specimens corroded considerably.

From this thesis work, following summary and conclusions can be made.

1. Compound formed on specimens after corrosion tests in gallium was observed to consist of primarily $FeGa_3$ with some $CrGa_4$ and Ni_2Ga3. Grain-boundary attack was not found at the interface between gallium and specimen. It is possible that ternary and quaternary compounds also formed.

2. Specimens tested in gallium alloy environments (Ga-14Sn-6Zn and Ga-8Sn-6Zn), 1~2 wt% of zinc was observed in the reaction layer near the interface. Zinc can be compounded with iron.

3. The weight change of bare specimens that exposed to gallium alloys is smaller than that exposed to pure gallium.

4. The pre-oxidized specimens that exposed to gallium and Ga-8Sn-6Zn environments gained their weight more than that of bare specimens. Pre-oxidized specimens that exposed to Ga-14Sn-6Zn environment gained more in air condition and lost more in vacuum conditions compared to bare specimens.

5. General behavior of developing reaction layer within the effect of pre-oxidation is that pre-oxidized specimens, in any conditions, had developed as thick as reaction layers on bare specimens.

For future work,

1. The commercial equipment for active control of oxygen partial pressure could not realize lower oxygen partial pressure than $1.356*10^{-38}$ atm. For the stable formation of protective oxide scale, the oxygen partial pressure should be set the order of $10^{-40} \sim 10^{-41}$ atm. In real time, the oxygen partial pressure can be monitored by yttrium stabilized zirconia (YSZ) oxygen sensor.

2. It is possible that other protective oxide scales can be applied to the surface of SS 316L in gallium and gallium alloys environments. SiO_2 and Al_2O3 can be coated by several coating techniques or formed on the surface of alloys that have silicon and aluminum contents and the forming principles are the same as described in this thesis.

Acknowledgements

During my stay at UNIST, I have met many people those who gave good impacts to my life.

I am deeply grateful my thesis advisor, Professor Ji Hyun Kim, for his guidance and unwavering support to me throughout my stay at UNIST. He has always supported my research work. I owe special thanks to my thesis committee members, Professor Yonghee Kim and Professor In Cheol Bang for their advice that helped me bring my research to final fruition.

Special thanks must be given to Dr. Mi Jung Jin and Ms. Jae Eun Yu, for their sincere help for EPMA. I would also like to thank the research staff of the UNIST Central Research Facility (UCFR), especially Mr. Dong Ju Lim and Mr. Young Gi Kim for their training and help with important materials characteristic tools including SEM and sample preparations.

I sincerely thank to my laboratory colleague, Seung Won Lee, Jong Jin Kim, Jeong Seok Park, Sung Dae Park, Sa Rah Kang, Ju Ang Jeong, and Seung Hyun Kim for sharing our joys and sorrows.

This work has been supported by Nuclear Research & Development Program through the National Research Foundation of Korea (NRF) funded by the Ministry of Education, Science and Technology.

None of this would have been possible without prayer of my parents who have always stood by my side with their never-ending love and unshakable trust in me. I owe them so much.